PALEOANTHROPOLOGY

The earliest modern humans outside Africa

Israel Hershkovitz,[1,2]*† Gerhard W. Weber,[3]† Rolf Quam,[4,5,6]† Mathieu Duval,[7,8] Rainer Grün,[7,9] Leslie Kinsley,[9] Avner Ayalon,[10] Miryam Bar-Matthews,[10] Helene Valladas,[11] Norbert Mercier,[12] Juan Luis Arsuaga,[5,13] María Martinón-Torres,[8,14] José María Bermúdez de Castro,[8,14] Cinzia Fornai,[3,15] Laura Martín-Francés,[8,16] Rachel Sarig,[2,17] Hila May,[1,2] Viktoria A. Krenn,[3,15] Viviane Slon,[1] Laura Rodríguez,[5,18,19] Rebeca García,[5,18] Carlos Lorenzo,[20,21] Jose Miguel Carretero,[5,18] Amos Frumkin,[22] Ruth Shahack-Gross,[23] Daniella E. Bar-Yosef Mayer,[24,25] Yaming Cui,[26] Xinzhi Wu,[26] Natan Peled,[27] Iris Groman-Yaroslavski,[28] Lior Weissbrod,[28] Reuven Yeshurun,[28] Alexander Tsatskin,[28] Yossi Zaidner,[28,29] Mina Weinstein-Evron[28]

To date, the earliest modern human fossils found outside of Africa are dated to around 90,000 to 120,000 years ago at the Levantine sites of Skhul and Qafzeh. A maxilla and associated dentition recently discovered at Misliya Cave, Israel, was dated to 177,000 to 194,000 years ago, suggesting that members of the *Homo sapiens* clade left Africa earlier than previously thought. This finding changes our view on modern human dispersal and is consistent with recent genetic studies, which have posited the possibility of an earlier dispersal of *Homo sapiens* around 220,000 years ago. The Misliya maxilla is associated with full-fledged Levallois technology in the Levant, suggesting that the emergence of this technology is linked to the appearance of *Homo sapiens* in the region, as has been documented in Africa.

The timing and routes of modern human migration out of Africa are key issues for understanding the evolution of our own species. The fossil evidence suggests that the earliest members of the *Homo sapiens* clade (Jebel Irhoud, Omo, and Herto) appeared in Africa during the late Middle Pleistocene (*1*–*4*). Outside Africa, modern humans appeared much later, during the Late Pleistocene in the Levant (Qafzeh, Skhul) (*5*–*7*), and possibly in East Asia (Daoxian) (*8*). Misliya Cave, Israel, is part of a complex of prehistoric caves along the western slopes of Mount Carmel (Fig. 1 and fig. S1). Here we report on an adult hominin left hemimaxilla (Misliya-1) (Fig. 2A) found in Square N9 of the upper part of the Early Middle Palaeolithic (EMP) archaeological layer of the site (Stratigraphic Unit 6, Upper Terrace, Fig. 1 and fig. S1), associated with an Early Levantine Mousterian (Tabun D type) stone-tool assemblages (*9*, *10*). Misliya-1 preserves much of the alveolar and zygomatic processes, part of the palate and nasal floor, and the complete left dentition from the first incisor (represented by a broken root only) to the third molar (Fig. 2A).

Three independent numerical dating methods—U-series (U-Th), combined uranium series and electron spin resonance (US-ESR) series, and thermoluminescence (TL)—carried out in three different dating laboratories yielded consistent results (Fig. 2B, figs. S2 and S3, and tables S1 and S3). A series of nine TL dates on burnt flints from Square L10 and N12 in the vicinity of the human fossil (Fig. 1, A and B) provided a mean age of 179 ± 48 thousand years (ky) (2σ) (range = 212 to 140 ky) (*11*). U-Th analyses of the dentine of the I^2 from the maxilla and of the crust adhering directly to the maxilla yielded a minimum age of 70.2 ± 1.6 ky (2σ; table S1) and 185 ± 8.0 ky (2σ; Fig. 2B and table S2), respectively (*9*). The combined US-ESR dating of the enamel of the same tooth yielded a maximum age of 174 ± 20 ky (2σ)

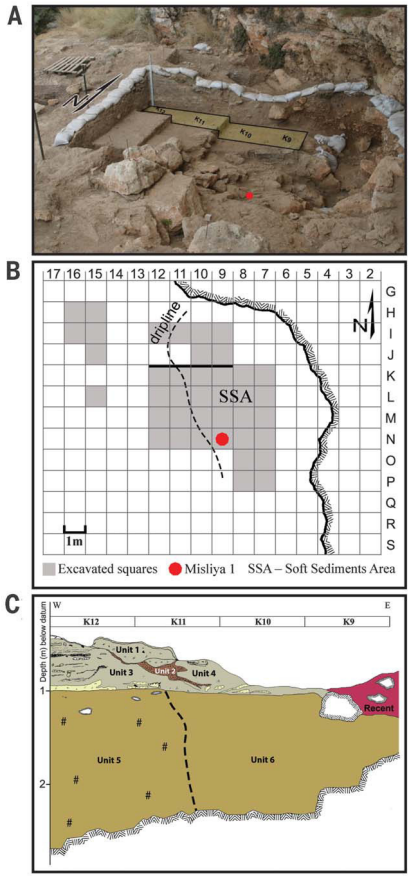

Fig. 1. The Misliya Cave excavation area at the Upper Terrace of the cave and the stratigraphy. (**A**) The excavation area and the location of the Misliya-1 maxilla (red dot). Squares K9 to K12 are indicated. (**B**) Map of the Misliya Cave Upper Terrace excavations (1 m^2 grid) with denoted excavated squares and showing the location of the human maxilla (Misliya-1). (**C**) Stratigraphic section of the Upper Terrace, squares K9 to K12. Apart from Unit 2, a Terra Rosa soil intrusion, all units contain EMP finds or assemblages. The present-day dripline roughly separates between highly cemented (Units 1,3,5) and more loosely cemented (Units 4 and 6) sediments. Misliya-1 was retrieved from the upper part of Unit 6.

[1]Department of Anatomy and Anthropology, Sackler Faculty of Medicine, Tel Aviv University, Post Office Box 39040, Tel Aviv 6997801, Israel. [2]The Dan David Center for Human Evolution and Biohistory Research and The Shmunis Family Anthropology Institute, The Steinhardt Museum of Natural History, Tel Aviv University, Post Office Box 39040, Tel Aviv 6997801, Israel. [3]Department of Anthropology and Core Facility for Micro-Computed Tomography, University of Vienna, Althanstrasse 14, A-1090 Vienna, Austria. [4]Department of Anthropology, Binghamton University (SUNY), Binghamton, NY 13902-6000, USA. [5]Centro UCM-ISCIII de Evolución y Comportamiento Humanos, Avda. Monforte de Lemos, 5, 28029, Madrid, Spain. [6]Division of Anthropology, American Museum of Natural History, Central Park West at 79th Street, New York, NY 10024-5192, USA. [7]Australian Research Centre for Human Evolution (ARCHE), Environmental Futures Research Institute, Griffith University, Nathan QLD 4111, Australia. [8]National Research Center on Human Evolution (CENIEH), Paseo de la Sierra de Atapuerca 3, 09002, Burgos, Spain. [9]Research School of Earth Sciences, The Australian National University, Canberra ACT 2601, Australia. [10]Geological Survey of Israel, 30 Malkhe Israel Street, Jerusalem 9550161, Israel. [11]Laboratoire des Sciences du Climat et de l'Environnement, LSCE/IPSL, CEA-CNRS-UVSQ, Université Paris-Saclay, avenue de la terrasse, 91198 Gif sur Yvette Cedex, France. [12]Institut de Recherche sur les Archéomatériaux, UMR 5060 CNRS - Université de Bordeaux Montaigne, Centre de Recherche en Physique Appliquée à l'Archéologie (CRP2A), Maison de l'archéologie, 33607 PESSAC Cedex, France. [13]Departamento de Geodinámica, Estratigrafía y Paleontología, Facultad de Ciencias Geológicas, Universidad Complutense de Madrid, Ciudad Universitaria s/n, 28040, Madrid, Spain. [14]Department of Anthropology, University College London, 14 Taviton Street, London, WC1H 0BW, UK. [15]Institute of Evolutionary Medicine, University of Zurich, Winterthurerstrasse 190, CH-8057 Zurich, Switzerland. [16]UMR5189 PACEA Université de Bordeaux, CNRS MCC, France. [17]Department of Oral biology and Orthodontics, the Maurice and Gabriela Goldschleger School of Dental Medicine, Sackler Faculty of Medicine, Tel Aviv University, 6997801 Israel. [18]Departamento de Historia, Geografía y Comunicación, Universidad de Burgos, Facultad de Humanidades y Comunicación, 09001, Burgos, Spain. [19]Facultade de Humanidades, Universidad Isabel I, Spain. [20]Área de Prehistoria, Universitat Rovira i Virgili, Avinguda Catalunya 35, 43002 Tarragona, Spain. [21]Institut Català de Paleoecologia Humana i Evolució Social (IPHES), Marcel·lí Domingo s/n, 43007 Tarragona, Spain. [22]Institute of Earth Science, The Hebrew University of Jerusalem, Jerusalem 9190401, Israel [23]Department of Maritime Civilizations, Recanati Institute of Maritime Studies, University of Haifa, Haifa, Mount Carmel 3498838, Israel. [24]Sonia and Marco Nadler Institute of Archaeology Tel Aviv University, Tel Aviv 69978, Israel. [25]Peabody Museum of Archaeology and Ethnology, Harvard University, 11 Divinity Avenue, Cambridge, MA 02138, USA. [26]Department of Paleoanthropology, Institute of Paleontology and Paleoanthropology, Chinese Academy of Science, Str. Xizhimenwai no. 144, 100044 Beijing, China. [27]Department of Radiology, Carmel Medical Center, Haifa, 3436212 Israel. [28]Zinman Institute of Archaeology, University of Haifa, Haifa, Mount Carmel 3498838, Israel. [29]Institute of Archaeology, The Hebrew University of Jerusalem, Jerusalem 9190501, Israel.
***Corresponding author. Email: anatom2@tauex.tau.ac.il** †These authors contributed equally to this work.

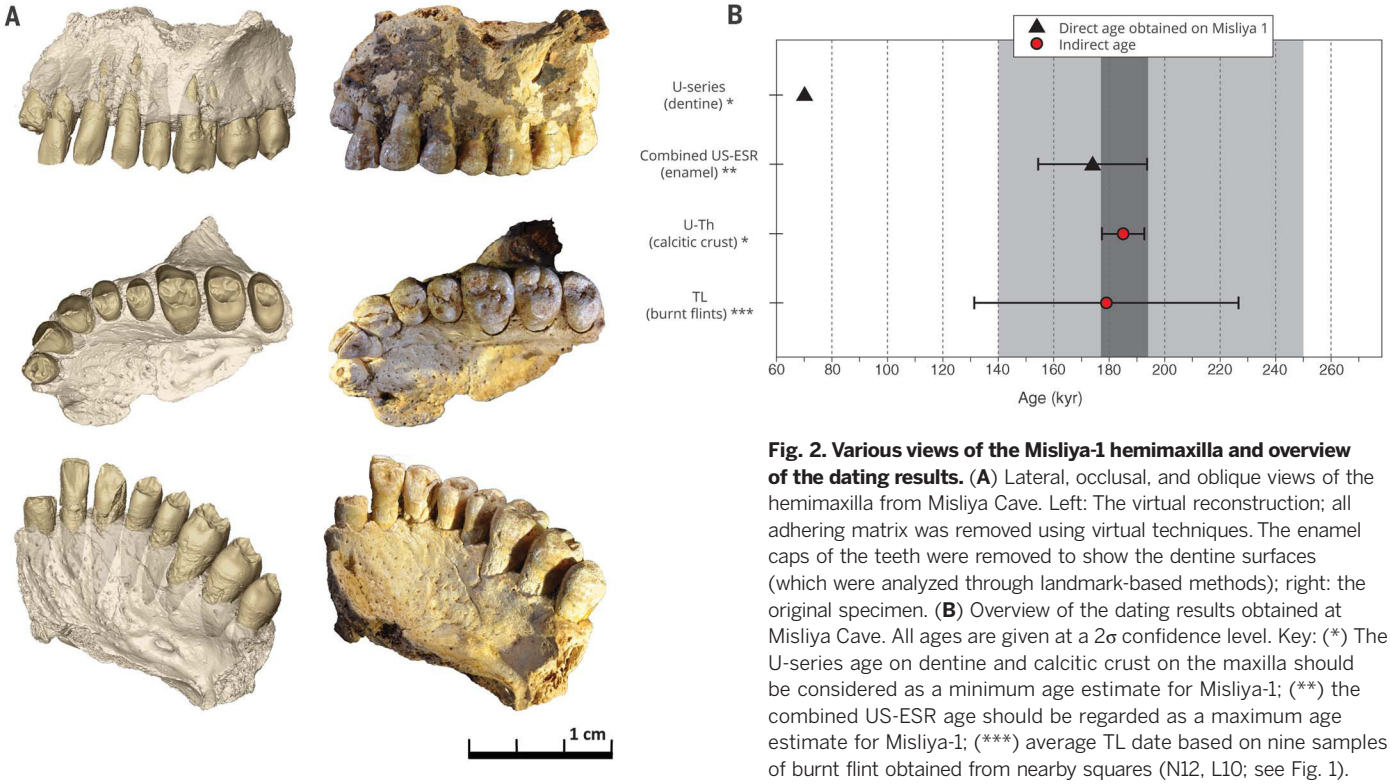

Fig. 2. Various views of the Misliya-1 hemimaxilla and overview of the dating results. (**A**) Lateral, occlusal, and oblique views of the hemimaxilla from Misliya Cave. Left: The virtual reconstruction; all adhering matrix was removed using virtual techniques. The enamel caps of the teeth were removed to show the dentine surfaces (which were analyzed through landmark-based methods); right: the original specimen. (**B**) Overview of the dating results obtained at Misliya Cave. All ages are given at a 2σ confidence level. Key: (*) The U-series age on dentine and calcitic crust on the maxilla should be considered as a minimum age estimate for Misliya-1; (**) the combined US-ESR age should be regarded as a maximum age estimate for Misliya-1; (***) average TL date based on nine samples of burnt flint obtained from nearby squares (N12, L10; see Fig. 1). Dark gray: Age range for Misliya-1, based on dates obtained from the fossil (U-Th provides the minimum age and combined US-ESR the maximum age), is between 177 ky (=185 – 8 ky) to 194 ky (=174 + 20 ky). Light gray: Age range for the EMP period in the Levant (250 to 140 ky) based on the combination of TL dates obtained for Tabun Cave (*13*), Hayonim Cave (*12*), and Misliya Cave (*11*).

(Fig. 2B, fig. S3, and tables S1 and S3) (*9*). All these dates, except for the U-series dating of the dentine, which exclude the possibility of recent intrusion, fall within the time range for the Early Levantine Mousterian lithic industry (Tabun D-type) observed at Tabun, Hayonim, and Misliya caves (i.e., ~250 to ~140 ky) (*11*–*13*) and are older than the upper range defined for the EMP sequence in Misliya Cave (>165 ky) (*11*). Collectively, the evidence suggests an early marine isotope stage 6 (MIS 6) age for the Misliya-1 fossil. The age range for Misliya-1, based on dates directly connected with the fossil (U-Th on crust providing the minimum boundary and the maximum boundary of US-ESR on the enamel of I^2), is between 177 and 194 ky [for details and calculation methods, see (*9*) and fig. S2].

The insertion of the zygomatic root in Misliya-1 is relatively anteriorly placed, at the level of M^1, similar to recent *H. sapiens* as well as the fossils from Herto and Jebel Irhoud (*1*, *3*). The zygomaticoalveolar crest is strongly curved and inserts at a low position relative to the dentition. Three-dimensional (3D) geometric morphometric (GM) analysis (*9*) of the maxillary morphology (Fig. 3A) shows that Misliya-1 is similar to modern humans and is most dissimilar to Neandertals and some Middle Pleistocene hominins. Based on the logarithm of the centroid size of the 3D data (*9*), Misliya-1 is smaller than all fossil *Homo* specimens in our sample and falls in the range of variation observed for recent modern humans. In addition, the anterior placement of the incisive foramen, the sloped or level nasal floor configuration, and the shape of the dental arcade in Misliya-1 (Fig. 2A) are characteristic of modern humans, although individual features can occasionally be found in earlier taxa.

The I^2 (Fig. 2A and fig. S4) shows several features that are characteristic of *H. sapiens* (*14*), including a flat labial surface [labial convexity grades 0 or 1, scoring based on Arizona State University Dental Anthropology System (ASUDAS)], a straight incisal edge, very slight shoveling (ASUDAS grade 1), and lack of a lingual tubercle. The presence of a lingual groove can also be found in Pleistocene *H. sapiens* samples such as Qafzeh and Huanglong. The canine lacks the mass-additive traits typical of Asian *Homo erectus* (*15*), Middle Pleistocene European specimens, and Neandertals, and resembles Qafzeh and Skhul. Unlike Neandertals canines, the shovel shape is not pronounced, and there is no lingual tubercle or mesial canine ridge (Fig. 2A).

The upper premolars display relatively simple occlusal surfaces and lack accessory marginal tubercles and buccal cingulum (Fig. 2A). The Misliya-1 premolars display the typical high and narrow crown of *H. sapiens*. In the occlusal view, the P^3 shows a slight lingual narrowing, which is less pronounced in the P^4. This contrasts with the characteristic Neandertal pattern featuring a low and broad crown and subequal buccal and lingual aspects of the crown in both upper premolars. The proportion of occlusal area (defined by the occlusal rim) is large relative to the crown base area in the upper premolars of Misliya-1, unlike in Neandertals, where the occlusal area appears compressed relative to the crown base area. This compression in Neandertal upper premolars is homologous to the relative reduction of the occlusal polygon found in Neandertal M^1s (*16*, *17*), and this latter feature is absent in Misliya-1.

The Misliya-1 maxillary teeth are within the upper size range of modern humans (table S5). Size proportions between the anterior and posterior teeth differentiate Misliya-1 from Neandertals (fig. S5). The buccolingual (BL) size ratio of the I^2 to M^1 in Misliya-1 (62.6) is just outside the upper limit of the range of modern humans (mean = 55.6, SD = 3.4, n = 31, range = 48.2 to 62.5), is similar to the mean of Qafzeh and Skhul (mean = 63.4, SD = 4.9, n = 9, range = 56.1 to 71.4), and well below the lower limit of the range of Neandertals (mean = 70.3, SD = 3.1, n = 13, range = 66.7 to 76.0). Therefore, Misliya-1 does not exhibit the relative expansion of the anterior dentition characteristic of Neandertals (*18*). Tooth root size and morphology are also within the range of modern humans (fig. S4).

Two-dimensional GM analysis (*9*) of the M^1 crown outline (Fig. 4) reveals that Misliya-1 is separate from Neandertals and other European Middle Pleistocene hominins, placing it with modern humans and near to Jebel Irhoud. It differs from Neandertals as well as from other European Middle Pleistocene fossils by not displaying the skewed rhomboidal crown outline

and large and protruding hypocone. The relative sizes of the M^1 protocone and hypocone align Misliya-1 with modern humans and differentiate it from Neandertals (table S4).

The 3D GM analysis (*9*) of the premolars, including the enamel-dentine junction (EDJ) occlusal area and cementum-enamel junction (CEJ) (fig. S6), shows that the Misliya-1 premolars are located in quadrants exclusively occupied by *H. sapiens*, with the exception of one Atapuerca Sima de los Huesos (SH) P^3 (that is located in the same quadrant but far from Misliya-1) and the P^4 of Amud 1. A similar analysis of the Misliya-1 M^2 (Fig. 3B) places it in an area exclusively occupied by contemporary *H. sapiens* (and the Liujiang specimen), which are characterized by a reduction of the hypocone and a buccolingually widened (rectangular) crown base. This contrasts with what is observed in Neandertals and most other European Middle Pleistocene fossils where the hypocone is relatively more developed. The Qafzeh specimens are quite variable but uniformly display a larger hypocone than does Misliya-1. The strong reduction of the hypocone observed in M^1 (table S4), M^2, and M^3 of Misliya-1 is most frequently observed in *H. sapiens*, although it can occasionally be found in other *Homo* groups (*17*, *18*).

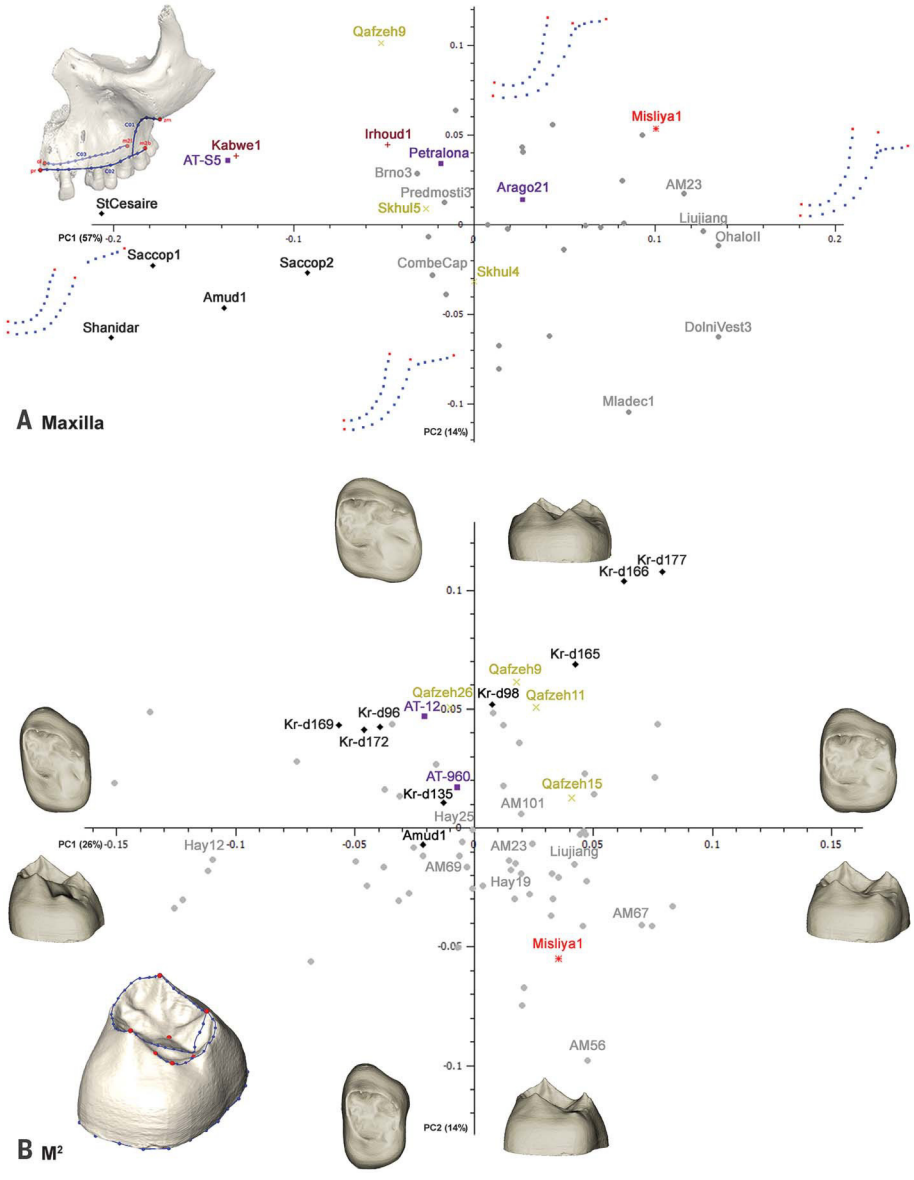

Fig. 3. First two principal components (PCs) in shape space and associated warped surfaces at the extremities of the axes. Noteworthy shape changes in the warpings are as follows: (**A**) Maxillary bone. PC1, anterior-posterior position and angle of the zygomatic root. PC2, curvature of the zygomatico-alveolar crest. (**B**) Upper M^2; PC2, relative expansion and height of the hypocone; buccolingual relative size of the EDJ occlusal area to the crown base. On the left side of each of the plots, the landmark configurations used for the respective anatomical unit are represented (landmarks in red, curve semilandmarks and pseudolandmarks on CEJ in blue). Prosthion (pr), orale (ol), zygomaxillare (zm), midpoint of the M^2 alveolar socket buccally (m2b) and lingually (m2l); upper region of the zygomaticoalveolar crest (C01); buccal alveolar margin (C02), lingual alveolar margin (C03). Red star, Misliya-1; gray circles, recent modern humans (without labels), Upper Paleolithic and Epipaleolithic modern *Homo* (with labels); black diamonds, Neandertals; yellow X, early modern humans; violet square, European Early and Middle Pleistocene *Homo*; burgundy plus sign, African Early and Middle Pleistocene *Homo*; for the specimen labels, refer to table S7.

Overall, the Misliya-1 teeth are distinct from those of the Middle Pleistocene specimens from Europe, Africa, and Asia such as Atapuerca (SH), Steinheim, Rabat, Qesem Cave, Chaoxian, and Xujiayao. Although some dental features seen in Misliya-1 can occasionally also be found in some of these samples, the entire suite of metric and morphological traits seen in the Misliya-1 maxillary bone and teeth is more consistent with *H. sapiens* than with Neandertals or other Middle Pleistocene hominin groups. Indeed, the combination of features in the incisor and canine appears to occur only in *H. sapiens* (*19*).

Middle Pleistocene fossils from southwest Asia (e.g., Qesem Cave, Zuttiyeh) are rare and display a mixture of features considered characteristic of Neandertals or modern humans, thus complicating their taxonomic assignment (*20*–*22*). Although incomplete, the Misliya-1 maxilla does not exhibit any derived skeletal or dental Neandertal features. A specific comparison with the earlier teeth from Qesem Cave (*20*, *21*) reveals a number of differences. Specifically, the Qesem I^2 shows a pronounced lingual tubercle, greater degree of labial curvature, and more pronounced shoveling, whereas the Qesem C^1 shows more pronounced shoveling, a lingual tubercle, and a canine mesial ridge. All of these features are more commonly found in Neandertal anterior teeth and represent points of departure from the morphology seen in Misliya-1 teeth. In contrast, Misliya-1 resembles the later Levantine *H. sapiens* fossils from the sites of Skhul and Qafzeh regarding many dental features, but it also differs from them regarding the degree of hypocone reduction seen in Misliya-1.

The geographical origin, timing, and identification of the last common ancestor of Neandertals and modern humans remain controversial (*23*, *24*). Nevertheless, the evolutionary emergence of Neandertals in Europe from their Middle Pleistocene precursors [e.g., Atapuerca (SH), Steinheim, Ehringsdorf] is better established, despite the possibility that more than one lineage coexisted in the European Middle Pleistocene (*25*). The geographical origin of *H. sapiens* is generally considered to be Africa, and the Jebel Irhoud fossils, recently dated to ~300 ky ago (*2*), are thought to represent an "early phase of *H. sapiens* evolution" [(*1*), p. 291]. Younger fossils from the sites of Omo (~195 ky ago) and Herto (~160 ky ago) have been attributed to *H. sapiens* (*3*, *4*). Nevertheless, the African fossil records reveal temporal overlaps between more "archaic" and more "modern" forms of early *H. sapiens* (*24*). These African specimens are thought to be members of the *H. sapiens* clade, even though some of them fall outside the range

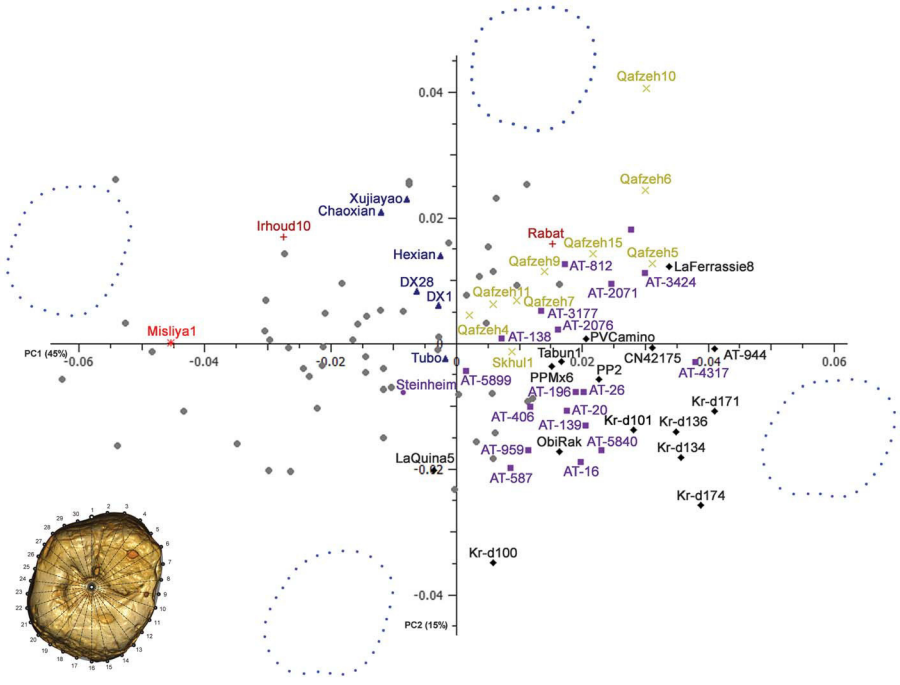

Fig. 4. First two principal components (PCs) of the crown shape of Misliya-1 M[1]. Misliya-1 is distinct from Neandertals and other Middle Pleistocene hominins and clearly grouped with modern humans. Red star, Misliya-1; gray circles, recent modern humans (without labels), Upper Paleolithic and Epipaleolithic modern *Homo* (with labels); black diamonds, Neandertals; yellow X, early modern humans; violet square, European Early and Middle Pleistocene *Homo*; burgundy plus sign, African Early and Middle Pleistocene *Homo*; blue triangle, Middle Pleistocene Asian specimens; for the specimen labels, refer to table S7.

of variation of Holocene humans regarding certain features (*3*, *24*). Similarly, many of the teeth, which are thought to represent early *H. sapiens* from North Africa, retain primitive features (*26*).

Misliya-1 considerably pushes back the timing of the earliest migration of members of the *H. sapiens* clade out of Africa, well predating Qafzeh and Skhul in the Levant, and Daoxian and Liujiang in China [(*8*) and (*27*); but see (*28*)].

Archaeologically, the EMP layers of Misliya cave document the emergence of novel technological concepts in the Levant, including full-fledged Levallois technology and laminar technology (*29*). Similar technological concepts have been documented at contemporary and earlier Middle Stone Age sites in Africa, i.e., the Maghreb (Jebel Irhoud), eastern Africa (Gademotta and Kulkuletti formations, Ethiopia, and the Kapthurin Formation, Kenya), and southern Africa (Kathu Pan) (*2*, *30*–*34*). Thus, similar to the recent findings from Jebel Irhoud (*1*, *2*), the evidence from Misliya Cave suggests that the emergence of full-fledged Levallois technology in the Levant may have also been associated with the occurrence of *H. sapiens*.

The region of southwest Asia represents a major biogeographic corridor for hominin migrations during our evolutionary history. Given the geographical proximity of the Levant to Africa, it is possible that the dispersals documented at Misliya Cave (177 to 194 ky ago), Qafzeh and Skhul Caves (90 to 120 ky ago), and Manot Cave (50 to 60 ky ago) reflect expansions of the geographical range of *H. sapiens*, fluctuating in response to demographic or environmental factors (*35*).

To date, Misliya-1 appears to represent the earliest fossil evidence of the migration of members of the *H. sapiens* clade out of Africa. It therefore opens the door to the possibility that *H. sapiens* dispersal from Africa could have occurred earlier than previously thought (probably before 200 ky ago), as has been recently suggested based on genetic evidence (*36*).

REFERENCES AND NOTES

1. J.-J. Hublin *et al.*, *Nature* **546**, 289–292 (2017).
2. D. Richter *et al.*, *Nature* **546**, 293–296 (2017).
3. T. D. White *et al.*, *Nature* **423**, 742–747 (2003).
4. I. McDougall, F. H. Brown, J. G. Fleagle, *Nature* **433**, 733–736 (2005).
5. N. Mercier *et al.*, *J. Archaeol. Sci.* **20**, 169–174 (1993).
6. C. B. Stringer, R. Grün, H. P. Schwarcz, P. Goldberg, *Nature* **338**, 756–758 (1989).
7. H. P. Schwarcz *et al.*, *J. Hum. Evol.* **17**, 733–737 (1988).
8. W. Liu *et al.*, *Nature* **526**, 696–699 (2015).
9. Materials and methods are available as supplementary materials online.
10. Y. Zaidner, M. Weinstein-Evron, *Before Farm.* **2012**, 1–23 (2012).
11. H. Valladas *et al.*, *J. Hum. Evol.* **65**, 585–593 (2013).
12. N. Mercier *et al.*, *J. Archaeol. Sci.* **34**, 1064–1077 (2007).
13. N. Mercier, H. Valladas, *J. Hum. Evol.* **45**, 401–409 (2003).
14. M. Martinón-Torres *et al.*, *Proc. Natl. Acad. Sci. U.S.A.* **104**, 13279–13282 (2007).
15. F. Weidenreich, *The dentition of* Sinanthropus pekinensis; *a comparative odontography of the hominids. Palaeontol Sinica, New Series D1* (Peking, 1937).
16. S. E. Bailey, *J. Hum. Evol.* **47**, 183–198 (2004).
17. M. Martinón-Torres, J. M. Bermúdez de Castro, A. Gómez-Robles, L. Prado-Simón, J. L. Arsuaga, *J. Hum. Evol.* **62**, 7–58 (2012).
18. J. M. Bermúdez de Castro, M. E. Nicolas, *Am. J. Phys. Anthropol.* **96**, 335–356 (1995).
19. S. E. Bailey, J. Hublin, in *Anthropological Perspectives on Tooth Morphology: Genetics, Evolution, Variation*, G. Scott, J. Irish, Eds. (Cambridge Univ. Press, Cambridge, 2013), pp. 222–249.
20. G. Weber *et al.*, *Quat. Int.* **398**, 159–174 (2016).
21. I. Hershkovitz *et al.*, *Am. J. Phys. Anthropol.* **144**, 575–592 (2011).
22. S. E. Freidline, P. Gunz, I. Janković, K. Harvati, J.-J. Hublin, *J. Hum. Evol.* **62**, 225–241 (2012).
23. A. Gómez-Robles, J. M. Bermúdez de Castro, J.-L. Arsuaga, E. Carbonell, P. D. Polly, *Proc. Natl. Acad. Sci. U.S.A.* **110**, 18196–18201 (2013).
24. C. Stringer, *Philos. Trans. R. Soc. Lond. B Biol. Sci.* **371**, 1698 (2016).
25. J. L. Arsuaga *et al.*, *Science* **344**, 1358–1363 (2014).
26. S. E. Bailey, T. D. Weaver, J. Hublin, in *Human Paleontology and Prehistory*, A. Marom, E. Hovers, Eds. (Springer International, Cham, Switzerland, 2017), pp. 215–232.
27. G. Shen *et al.*, *J. Hum. Evol.* **43**, 817–829 (2002).
28. W. Liu, X. Wu, L. Wang, *Acta Anthropol. Sin.* **25**, 177–194 (2006).
29. M. Weinstein-Evron, Y. Zaidner, A. Tsatskin, R. Yeshurun, I. Hershkovitz, in *Quaternary of the Levant: Environments, Climate Change, and Humans*, Y. Enzel, O. Bar-Yosef, Eds. (Cambridge Univ. Press, Cambridge, 2017), pp. 225–230.
30. K. Douze, A. Delagnes, *J. Hum. Evol.* **91**, 93–121 (2016).
31. C. R. Johnson, S. McBrearty, *J. Hum. Evol.* **58**, 193–200 (2010).
32. N. Porat *et al.*, *J. Archaeol. Sci.* **37**, 269–283 (2010).
33. Y. Sahle, L. E. Morgan, D. R. Braun, B. Atnafu, W. K. Hutchings, *Quat. Int.* **331**, 6–19 (2014).
34. C. A. Tryon, S. McBrearty, P.-J. Texier, *Afr. Archaeol. Rev.* **22**, 199–229 (2005).
35. I. Hershkovitz *et al.*, *Nature* **520**, 216–219 (2015).
36. C. Posth *et al.*, *Nat. Commun.* **8**, 16046 (2017).

ACKNOWLEDGMENTS

Field work in Misliya Cave was supported by the Dan David Foundation, the Irene Levi-Sala CARE Archaeological Foundation, the Leakey Foundation, the Thyssen Foundation, and the Faculty of Humanities of the University of Haifa. Laboratory work and dating were supported by the Israel Science Foundation (grant no. 1104/12). The anthropological study was supported by the Dan David Foundation, Ministerio de Economía y Competitividad of Spain (CGL2015-65387-C3-2-3-P MINECO/FEDER), Fundación Atapuerca, and The Leakey Foundation. The ESR dating study received funding from the Marie Curie International Outgoing Fellowship (IOF) 626474 and the Australian Research Council Future Fellowship FT150100215. N.M. is grateful to LaScArBx ANR-10-LABX-52 for support. Work on the virtual specimens was supported by the Life Science Faculty University of Vienna; Oesterreichische Nationalbank, Anniversary Fund, project no. 16121; the Swiss National Science Foundation grant nos. 31003A 156299/1 and 31003A 176319; A.E.R.S. Dental Medicine Organizations GmbH, Vienna, Austria, project no. FA547014; and the Siegfried Ludwig–Rudolf Slavicek Foundation, Vienna, Austria, project no. FA547016. Special thanks are due to the late Dan David and his son, Ariel David, for their inspiration and financial support throughout the years. Thanks also go to O. Bar-Yosef (Harvard University) and A. M. Tillier (University of Bordeaux), who read and commented on a previous version of this paper. All data generated in this study are in the supplementary materials. Permission to study the fossil (Misliya-1) can be obtained from the corresponding author. Micro-CT images are available from G.W.W. under a material transfer agreement with I.H. of Tel Aviv University (Misliya-1). Full acknowledgments are in the supplementary materials. I.H. and M.W.-E. direct the Misliya Cave research project; I.H., G.W.W., R.Q., J.L.A., M.M.-T., J.M.B.dC., L.M.-F., P.S., R.S., H.M., V.S., L.R., R.G., C.L., J.M.C., Y.C., X.W., and N.P. carried out various aspects of the anthropological study of the Misliya human remains; G.W.W., C.F., V.A.K., and R.S carried out the virtual image manipulation and geometric morphometric investigations; Y.Z. and M.W.-E. conducted the archaeological studies at the cave; A.A and M.B.-M. conducted the U/Th analysis; H.V. and N.M. conducted the TL dating of the archaeological layers; M.D., R.G., and L.K. conducted the U-series and ESR dating of the fossil remains; A.F., R.S.-G., and A.T. conducted the geoarchaeological and geomorphological studies of the cave; L.W. and R.Y. conducted the study of the faunal remains; D.B.-Y.M. studied the mollusc shells; and I.G.-Y. carried out the use-wear analysis. All authors participated in compiling the manuscript. The authors declare no competing financial interests.

SUPPLEMENTARY MATERIALS

www.sciencemag.org/content/359/6374/456/suppl/DC1
Materials and Methods
Supplementary Text
Acknowledgments
Figs. S1 to S6
Tables S1 to S7
References (*37*–*114*)

31 August 2017; accepted 21 December 2017
10.1126/science.aap8369

Science

The earliest modern humans outside Africa

Israel Hershkovitz, Gerhard W. Weber, Rolf Quam, Mathieu Duval, Rainer Grün, Leslie Kinsley, Avner Ayalon, Miryam Bar-Matthews, Helene Valladas, Norbert Mercier, Juan Luis Arsuaga, María Martinón-Torres, José María Bermúdez de Castro, Cinzia Fornai, Laura Martín-Francés, Rachel Sarig, Hila May, Viktoria A. Krenn, Viviane Slon, Laura Rodríguez, Rebeca García, Carlos Lorenzo, Jose Miguel Carretero, Amos Frumkin, Ruth Shahack-Gross, Daniella E. Bar-Yosef Mayer, Yaming Cui, Xinzhi Wu, Natan Peled, Iris Groman-Yaroslavski, Lior Weissbrod, Reuven Yeshurun, Alexander Tsatskin, Yossi Zaidner and Mina Weinstein-Evron

Science **359** (6374), 456-459.
DOI: 10.1126/science.aap8369

Earliest modern humans out of Africa

Recent paleoanthropological studies have suggested that modern humans migrated from Africa as early as the beginning of the Late Pleistocene, 120,000 years ago. Hershkovitz *et al.* now suggest that early modern humans were already present outside of Africa more than 55,000 years earlier (see the Perspective by Stringer and Galway-Witham). During excavations of sediments at Mount Carmel, Israel, they found a fossil of a mouth part, a left hemimaxilla, with almost complete dentition.

The sediments contain a series of well-defined hearths and a rich stone-based industry, as well as abundant animal remains. Analysis of the human remains, and dating of the site and the fossil itself, indicate a likely age of at least 177,000 years for the fossil—making it the oldest member of the *Homo sapiens* clade found outside Africa.

Science, this issue p. 456; see also p. 389

Science (print ISSN 0036-8075; online ISSN 1095-9203) is published by the American Association for the Advancement of Science, 1200 New York Avenue NW, Washington, DC 20005.

www.sciencemag.org/content/359/6374/456/suppl/DC1

Supplementary Materials for

The earliest modern humans outside Africa

Israel Hershkovitz,* Gerhard W. Weber, Rolf Quam, Mathieu Duval, Rainer Grün, Leslie Kinsley, Avner Ayalon, Miryam Bar-Matthews, Helene Valladas, Norbert Mercier, Juan Luis Arsuaga, María Martinón-Torres, José María Bermúdez de Castro, Cinzia Fornai, Laura Martín-Francés, Rachel Sarig, Hila May, Viktoria A. Krenn, Viviane Slon, Laura Rodríguez, Rebeca García, Carlos Lorenzo, Jose Miguel Carretero, Amos Frumkin, Ruth Shahack-Gross, Daniella E. Bar-Yosef Mayer, Yaming Cui, Xinzhi Wu, Natan Peled, Iris Groman-Yaroslavski, Lior Weissbrod, Reuven Yeshurun, Alexander Tsatskin, Yossi Zaidner, Mina Weinstein-Evron

*Corresponding author. Email: anatom2@tauex.tau.ac.il

Published 26 January 2018, *Science* **359**, 456 (2018)
DOI: 10.1126/science.aap8369

This PDF file includes:

Materials and Methods

The Misliya-1 maxilla

Misliya-1 maxilla is housed at the anthropological collection of the Dan David Center for Human Evolution and Biohistory Research, Tel Aviv University.

When discovered, Misliya-1 was encapsulated by cemented sediments that were almost completely removed (with the exception of a fragment adhering to the root of the zygomatic process). The remaining cemented patch was eliminated via virtual techniques before the morphometric analysis. The slight degree of wear on the posterior dentition and the closed root apices on the M^3 suggest a young adult individual.

The Misliya-1 specimen (Fig. 2A) consists of a partial left hemi-maxilla, preserving most of the alveolar portion and the root of the zygomatic process. A portion of the hard palate is preserved, including the incisive foramen and part of the midline intermaxillary suture. The floor of the maxillary sinus is exposed, and the nasal floor is partially preserved with the lateral portion extending posteriorly to the level of the M^3. Anterior to this, the break runs obliquely towards the midline and the lateral 2/3 of the nasal floor is preserved anteriorly. The nasal floor continues anteriorly up until the damaged (and missing) anterior nasal margin. The nasal spine is not preserved.

The I^2-M^3 are present in their alveolar sockets (Fig. 2A), but the I^1 is represented only by a portion of the root. All the teeth are fully formed and in functional occlusion. Tooth wear is slight, falling between stages C (18-22 years) and D (20-24 years) as defined by Lovejoy (37). The degree of wear on the Misliya-1 teeth is slightly more advanced than in the late adolescent/young adult Qafzeh 9, but compares favorably with that seen in the young adult Qafzeh 5 individual. The intermaxillary suture is unfused in

Misliya-1, but the timing of fusion in recent humans is variable, with even older individuals (>50 years) showing unfused sutures (38). Thus, the balance of the evidence suggests a young adult age for the Misliya-1 individual.

Comparative samples

The Misliya maxilla and teeth were compared morphologically and metrically with fossil and recent *H. sapiens* as well as Neanderthals. In addition, European, Asian and North African Middle Pleistocene hominins were included, given the geographic setting of Misliya Cave and the chronological results which place the fossil in the Late Middle Pleistocene. Comparisons with Early and Middle Pleistocene fossils attributed to *H. erectus/H. ergaster* were also made to help assess the phylogenetic polarity of certain features. Data for the comparative samples were either collected by the authors on original fossil specimens or taken from the literature. Maxillary and dental measurements for the recent human sample were taken on skeletal remains housed at Dan David Center for Human Evolution and Biohistory Research, Tel Aviv University. Measurements were also taken on Late Natufian and Neolithic maxillae and teeth from the southern Levant (ca. 13-8 ky BP). The sample compositions for the geometric morphometric (GM) analyses (2D and 3D) and I^2/M^1 ratio are given in table S7. Data for the M^1 cusp areas is mainly from Quam et al. (39) and Martinón-Torres et al. (40).

Morphology, size and shape of teeth and roots

The Arizona State University Dental Anthropology System (ASUDAS) (41) was used for scoring key dental morphological features. The crown mesiodistal (no. 81) and buccolingual (no. 81.1) dimensions were measured following Martin's definition (42). Total crown base area, absolute and relative cusp base areas, relative occlusal polygon

area, and cusp angles for M^1 were measured following Bailey (16) and Wood and Engleman (43). Root length of I^2 and C' were measured following Le Cabec et al. (44).

Geometric Morphometric comparative analysis of Misliya-1

Geometric morphometrics (GM) was used to compare the three-dimensional shape of the Misliya-1 maxillary bone and teeth (i.e., P^3, P^4, M^2), and two-dimensional shape of the M^1 with recent and Upper Paleolithic human populations, early modern humans, Neanderthals, Middle Pleistocene *Homo*, and some early *Homo*. The side showing a better state of preservation was used for both maxilla and teeth and all right-sided specimens were mirror-imaged to the left. All data operations followed the guidelines for Virtual Anthropology (45). Misliya-1 was scanned at the Core Facility for Micro-Computed Tomography at the University of Vienna with a custom built VISCOM X8060 (Germany) µCT scanner: 130kV, 200µA, 1400msec, diamond high performance transmission target, 0.5mm copper filter, spatial resolution 28.2µm. X-ray images were taken from 1440 different angles. Using filtered back-projection in VISCOM XVR-CT 1.07 software, these data were reconstructed as 3D volumes with a color depth of 16,384 grey values.

Landmark collection on the maxillary bone

Landmarks Prosthion, Orale, Zygomaxillare, mid-point of the M^2 alveolar socket buccally and lingually were collected using Amira 6.0.1. (Mercury Computer Systems, Chelmsford, USA) and RapidForm XOR2 (INUS Technology), either from high resolution CT or µCT scans (resolution between 53-490µm) or from surface scans. For some individuals (table S7) only casts were available, therefore landmarks were sampled using a Microscribe 2GX device. Semilandmarks were placed on three curves, namely

along the superior portion of the zygomaticoalveolar crest (five semilandmarks), the lingual alveolar rim (ten semilandmarks), and the buccal alveolar rim (ten semilandmarks) and were slid using the minimum bending energy technique (46). The sliding process was performed in EVAN Toolbox 1.71 (http://evan-society.org).

3D landmark collection on teeth

High resolution CT or µCT scans (resolution between 8-70µm) were used. For the P^3, P^4, and M^2 we adapted the protocol recently published in Weber et al. (20). Pseudolandmarks were collected from the CEJ (47) and landmarks and curve semilandmarks from the EDJ occlusal area. These sets of landmarks were analyzed together. Separate analyses were carried out for each tooth type. Only teeth where these regions of interest were preserved were considered. Specimens affected by wear were included only if the dentine cusp(s) could be virtually reconstructed with confidence (therefore showing a degree of wear not higher than stage 3 according to Molnar (48).

The dentine was segmented from the enamel in Amira 6.0.1 using semi-automatic techniques. The 3D surface models of the EDJ were cropped at the best-fit plane of the cervical margins. Afterwards, they were imported into RapidForm XOR2 (INUS Technology), the cervical plane being parallel to the XY plane (47). Premolars were rotated so as to align the buccal ridge at the EDJ parallel with the X-axis. Molars were rotated so as to align their cervical mesial aspect parallel to the Y-axis. The CEJ outline was collected from each crown at the cervical plane and was imported in Rhinoceros 4.0 Beta CAD (Robert McNeel & Associates, Seattle, WA). The centroid for each outline area was calculated and 24 equiangularly (15^o) spaced radii originating from the centroid

were drawn. The intersection of the 24 radii with each of the outlines resulted in 24 pseudolandmarks describing the CEJ outlines of both molars and premolars.

Landmarks and curve semilandmarks were collected also on the EDJ occlusal area. Four landmarks were identified for P^3s and P^4s. For the P^3s (fig. S6), protocone dentine cusp tip, paracone dentine cusp tip, deepest point of the mesial fossa, and deepest point of the distal fossa were taken. In the case of the P^4s, since the last two landmarks were not consistently identifiable, we used instead the deepest point along the marginal edge of both mesial and distal margins. In case the marginal edge was straight, we took the mid-point. For both premolars, ten semilandmarks were collected on the mesial marginal ridge and ten semilandmarks on the distal marginal ridge. For the M^2s (Fig. 3B), seven landmarks were used: the dentine cusp tips of the protocone, paracone, metacone, hypocone, the deepest point of the central fossa, the deepest point of the distal fossa and the lowest point between the protocone and the hypocone along the marginal ridge. In addition, 43 curve semilandmarks were considered along the EDJ marginal ridge. Landmark collection and sliding were carried out using EVAN Toolbox 1.71. The occasional occurrence of additional cusps (e.g. cusp 5 on molars) is not captured by our protocol since all specimens in the data set need to possess the same number of homologous landmarks.

2D landmark collection on M^1s

Occlusal photographs of M^1s were rotated and aligned using Photoshop software according to the following protocol: buccal cusps oriented upwards and parallel to the X-axis, the buccal groove was positioned parallel to the Y-axis. Teeth that were damaged or extensively worn were excluded from the analysis. All left molars were

mirror imaged to the right, so all analyzed teeth were of right side. Crown outline was identified and digitized as a spline. In case of interproximal wear, the worn area was corrected using a pen tool in Photoshop software. The resulting outline was exported as a path to Rhinoceros 5 software (Robert McNeel & Associates, Seattle, Wash) where 30 pseudolandmarks were identified by crossing the outline with array of equiangular lines drawn from its centroid outwards, counting from the upper midbuccal point and clockwise. In case the image was taken from a micro-CT scan (different resolutions, different scanners, from multiple sources), the surfaces were first reconstructed in Amira 6.2.0 software (FEI software, Hillsboro, Oregon, USA), and then the best fit plane of the digitized CEJ curve was aligned parallel to XY plane. A screenshot was taken and the same protocol was used for alignment and measurement as described above. The landmark coordinates of all specimens were then transformed using Generalized Procrustes Analysis (with rotation disabled because the specimens were already rotated), and Principal Component Analysis of shape space (size disregarded, table S6) was performed using PAST 3.14 software (Ųyvind Hammer, Natural History Museum, University of Oslo).

GM analyses

Cartesian coordinates were converted into shape variables by means of a Generalized Procrustes Analysis (49, 50), which eliminates variation in orientation, location and size. Shape variables were then analyzed via Principal Component Analysis (PCA). Shape changes were visualized by Thin Plate Spline warping in EVAN Toolbox 1.71.

3D and 2D analyses

For the maxillary bone, P^3, P^4, and M^2 we used three-dimensional data based on landmarks and semilandmarks. These capture the actual geometry of the whole structure at once and thus represent a comprehensive image of the anatomical units in question (45). In particular, the combined data set for the teeth used here, consisting of the occlusal EDJ topography and the cervical outline (the base of the crown), accurately captures crown shape (see Fig. 3 and fig. S6) for the placement of landmarks and curves). The GM toolkit allows warping shape differences between specimens and groups using the Thin Plate Spline algorithm. It is thus possible to recognize where shape differences on a structure occur between individuals or groups, and the height of crowns and cusps is accurately included. One drawback of the approach is the limited sample size available for analysis since specimens with significant wear affecting the EDJ or showing fragmentation of the cervical rim cannot be used. This same limitation applies, to a lesser extent, to 2D analyses. Nevertheless, we added a 2D GM analysis of M^1 because this tooth type carries important taxonomic information. Since it is the first permanent tooth erupting in the upper jaw, its wear stage is most often beyond the limits for using 3D data of the EDJ. The 2D study for the M^1 includes a large and taxonomically diverse sample. It leads to the same conclusion as the 3D analyses, namely that Misliya-1 is unequivocally modern-like.

Uranium-series (U-series) and combined US-ESR dating of human fossil remains

Material

A fragment of enamel from the lateral incisor (sample #3532) and a bone fragment (sample #3533) were removed from the human maxilla (Misliya-1), which was found in the upper part of Unit 6 of the Upper Terrace.

Methods: U-series analysis

Laser ablation U-series analyses were carried out at the Research School of Earth Sciences of the Australian National University (Australia), using a custom-built laser sampling system interfaced between an ArF Excimer laser and a Finnigan Neptune Multi-collector Inductively Coupled Plasma Mass Spectrometer MC-ICP-MS (for details, see (51)), following principles and procedures described in Grün et al. (52). Tooth enamel and dentine were analyzed on separate lines. No individual age calculation was carried out when the U-concentrations were below about 0.5 ppm and/or detrital ^{232}Th was observed (elemental U/Th ratios below 300). The bone was analyzed along lines perpendicular to the outer surface on their cortical sections. For the tooth, the analytical data of the enamel and dentine sections were integrated to provide the data input for the ESR age calculations. U-series results are shown in table S1.

Methods: ESR measurements

An enamel fragment was extracted from the Misliya-1 lateral incisor (sample # 3532) and measured by ESR following the analytical procedure of Grün et al. (53). Doses were evaluated by a single aliquot additive dose method with a calibrated ^{137}Cs gamma source (dose rate = 7.05 Gy/min) using a sub-exponential dose step distribution with 0, 14, 42, 99, 212, 437, 861, 1707, 6263, 10495, 15574, 21923, 30388 and 36786 Gy. ESR measurements were carried out at the CENIEH (Burgos, Spain), with an EMXmicro 6/1 Bruker ESR spectrometer coupled to a standard rectangular ER 4102ST cavity. ESR measurements were performed at room temperature with the following acquisition parameters: 5-30 scans, 1 mW microwave power, 1024 points resolution, 15 mT sweep width, 100 kHz modulation frequency, 0.1 mT modulation amplitude, 20 ms conversion

time and 5 ms time constant. To ensure reproducible measurements, the fragment was mounted in a parafilm mould within a Teflon holder in a single position (53), which can be inserted into a Bruker ER 218PG1 programmable goniometer. Because the ESR signals of fragments show very strong angular dependences, ESR spectra were recorded in 10º increments over 360º for each dose step. ESR intensities were extracted from T1-B2 peak-to-peak amplitudes of the ESR signal of enamel, and normalized on the number of scans.

Methods: Dose evaluation

Fitting procedure was carried out with the Microcal OriginPro 9.1. software using a Levenberg-Marquardt algorithm by chi-square minimisation. Data were weighted by the inverse of the squared ESR intensity ($1/I^2$). D_E values were obtained by fitting the ESR intensities either with a single saturating exponential (SSE) or a double saturating exponential function (DSE) (54).

For the human enamel fragment 3532, ESR spectra were recorded in 10º increments over 360º for each dose step. Because of the preferential orientation of the hydroxyapatite crystals within the fragment, the shape and intensity of the ESR signal varies depending on the position of the fragment relative to the external magnetic field, which may affect the D_E value obtained for each angle (fig. S2). Dose Response Curves (DRCs) were obtained by merging the spectra of the different angles and measuring their T1-B2 intensities (fig. S2). The D_E values for the human tooth were derived from the DSE fitting procedure. For comparison, SSE fitting with $5<D_{max}/D_E<10$ as suggested by Duval and Grün (54) yield consistent D_E results within 1σ for sample #3532 (table S3).

Methods: Dose rate evaluation

For the dose rate calculations, the following parameters were used: an alpha efficiency of 0.13±0.02 (55), Monte-Carlo beta attenuation factors from Marsh (56), dose-rate conversion factors from Adamiec and Aitken (57), an estimated water content of 5±3 wt. % in dentine and 10±5 wt.% in sediment. Variations of the external dose rates within Unit 6 were assessed through a combination of *in situ* dosimetry measurements with thermoluminescence (TL) dosimeters and the collection of several complementary sediment samples. U, Th and K concentrations in raw sediment were determined by ICP-OES and ICP-MS analysis of the samples collected on site (table S3). These values were used for the external beta dose rate evaluation. We identified three TL dosimeters located within the upper part of Unit 6 in the vicinity of sample # 3532 that could be used to estimate the gamma dose rate. They provided values of 431, 359 and 368 µGy/a (11) yielding thus a mean gamma dose rate of 386±23 µGy/a (1 standard error). Valladas et al. (11) estimated the cosmic dose rate of 140 µGy/a for the samples of the upper part of Unit 6. A 5% relative error was assumed for the cosmic dose rate. Since it is not possible to remove an outer layer from the human tooth enamel, alpha doses from the sediment have to be considered. The external infinite matrix dose rate of a 50 µm thick enamel layer is 7.8% and 6.4% for the Th and U decay chains, respectively (58). Using the measured thicknesses of two fragments, the alpha efficiency and the sediment data, the average external alpha dose rates to the total enamel volume of both fragments is estimated to be less than 3 µGy/a.

Methods: Age calculation (US-ESR dating)

Combined US-ESR ages were calculated with USESR, a MATLAB-based program (59).

Results: U-series dating

U-series results on skeletal materials generally have to be regarded as minimum age estimates (52). The bone sample (sample # 3533) taken from the maxilla could not be dated because of high detrital ^{232}Th content (table S1). The tooth sample (# 3532) yielded a minimum age of 70.2±1.6 ky for the dentine, while no age could be obtained for the enamel given the very low U-concentration (<0.5 ppm; table S1).

Results: The role of thermally unstable gamma induced CO_2^- radicals in the ESR dose evaluation

Joannes-Boyau and Grün (60) showed that laboratory gamma irradiation may produce additional thermally unstable non-oriented CO_2^- radicals (NOCORs) compared to natural irradiation, which may lead to dose underestimations if this contribution is not removed. In contrast to enamel powder, fragment measurements allow the estimation of the relative distribution of NOCORs and anisotropic CO_2^- radicals (AICORs) (e.g., (53). We followed Method 3 of Joannes-Boyau (61) for the extraction of the NOCORs from the main radiation-induced ESR signal. Because of the AICORs, T1-B2 intensities vary over 360º reaching a maximum (I_{max}) and a minimum value (I_{min}) which are offset by about 90º (fig. S2). If the ratio of I_{max}/I_{min} is constant for each dose step, the relative distribution of NOCORs and AICORs is the same. However, it is often observed that the I_{max}/I_{min} ratio becomes smaller with increasing gamma doses, implying higher contributions of NOCORs in the overall ESR signal, which can be quantified from the change in the I_{max}/I_{min} ratios.

Sample 3532 (lateral incisor) shows a continuous decrease of I_{max}/I_{min} from 1.26 to 1.21, particularly over the first 400 Gy (fig. S2). This means that additional NOCORs

are created by gamma irradiation in 3532, the proportion of unstable NOCORs increasing from around 7% at 14 Gy to around 21% at 437 Gy (fig. S2); after that the relative NOCOR contribution remains more or less constant for doses of up 36 kGy. Assuming that all gamma induced NOCORs are unstable, the D_E value would increase by 26% (fig. S3 and table S3). However, Joannes-Boyau and Grün (60) argued that about half of the gamma-induced NOCORs convert into AICORs. Correcting for a 50% unstable NOCOR component, a D_E value of 112.6±1.8 Gy is obtained (12% higher than without correction), which we regard as the best dose estimate for sample 3532 (fig. S3 and table S3).

Results: Combined US-ESR age estimate

The human tooth (lateral incisor) fragment from the Misliya-1 maxilla yielded a combined US-ESR age of 174±10 ky (fig. S3). Because U-series data measured for the enamel were beyond secular equilibrium, the uptake parameter was fixed to -1 (assuming an Early Uptake), which generates the maximum dose possible for this tissue. This has, however, little impact on the final age result, as internal dose is less than 3% of the total dose rate. Because of the low U concentrations, the dental tissues actually contribute less than 5% to the total dose rate. The main issue with sample 3532 stems from the fact that the maxilla had been µCT-scanned three times in different institutions before the ESR dating analyses. Duval and Martin-Frances (62) recently showed that the magnitude of the X-ray dose given to the fossils during those µCT-scan experiments was highly variable, depending on the instrument and analytical procedure employed. For this reason, it is virtually impossible here to accurately assess the total X-ray dose absorbed by the tooth enamel of Misliya-1 during those µCT-scan analyses. As a consequence,

because the D_E value obtained for sample # 3532 may include a small contribution (of unknown magnitude) of this unwanted laboratory X-ray dose, the US-ESR age result of 174±10 ky should be regarded as a maximum possible estimate. In other words, the true age of the Misliya-1 maxilla is either similar to or younger than the US-ESR age obtained.

Summary: Age of the Misliya-1 specimen

No U-series age could be obtained for sample 3533 (bone fragment from the maxilla). In contrast, the age of the human tooth (#3532) from the Misliya-1 maxilla is constrained by a U-series age of 70.2±1.6 ky (table S1) and a combined US-ESR age of 174±10 ky (fig. S3) which should be considered as minimum and maximum possible ages, respectively.

U-Th dating of calcitic crust

Material

The studied sample includes calcitic crust covering the maxilla (Misliya-1) and archaeological artifacts derived from the same EMP layer. From the maxilla, 8 samples were collected from a small deposition under the zygomatic arch, other 13 samples were collected from crust depositions on animal bones or flints (table S2)**.** When discovered, the maxilla was covered by hard sediment, cleaned with acetic acid and washed using distilled water, in order to remove the covering sediment. A small chisel and a dental driller were used to take the samples. The calcite crusts were composed of authigenic calcite and authigenic and detrital clays evident by significant amounts of Si, Al, K.

Samples rich in detrital material were disaggregated in about 200 ml of distilled water using MISONIX XL2020 ultrasonic probe for about 2 minutes. The ultrasonification forced the clay-rich fine fraction into suspension and this fraction was decanted to remove it from the sample.

U-Th method

The Th dating techniques utilized and the age correction methods applied for the U-Th dates were described in detail in Hershkovitz et al (35).

U-Th dating was performed on 0.2-0.3 g of material. The powder was dissolved in 7M HNO_3 and HF, and a $^{229}Th/^{236}U$ spike was added. This solution was evaporated to dryness and dissolved in 4ml of 7M HNO_3. The solution was then loaded onto mini-columns that contained 2 ml Bio-Rad AG 1X8 200-400 mesh resin. U was eluted by 1M HBr and Th with 6M HCl, into different beakers. The U and Th beakers were placed on a hot plate set on 215ºC, and the solutions were evaporated to complete dryness and the residue dissolved in 2 ml and 5 ml of 0.1M HNO_3, respectively. U-Th dating was performed using a Nu Instruments Ltd (UK) Multi-Collector-Inductively-Coupled-Plasma-Mass-Spectrometer (MC-ICP-MS) equipped with 12 Faraday cups and 3 ion counters. Each sample was introduced to the MC-ICP-MS through an Aridus® micro-concentric desolvating nebulizer sample introducing system. The instrumental mass bias was corrected (using exponential equation) by measuring the $^{235}U/^{238}U$ ratio and correcting with the natural $^{235}U/^{238}U$ ratio. Calibration of ion counters relative to Faraday cups was performed using several cycles of measurement with different collector configuration in each particular analysis.

The main assumptions of the uranium-series dating method are that all ^{230}Th present in the calcite is formed *in-situ* by radioactive decay of U, and that the uranium-series radionuclide system is closed. However, initial ^{230}Th, which is the decay product of ^{234}U, can also be present in samples in association with the detrital component of the crusts. The detrital component may be composed of clays, alumino-silicates or Fe-oxyhydroxides with strongly absorbed Th^{4+} (35, 63, 64). The amount of ^{232}Th in the sample can be used as an indicator for the amount of contamination, since it is not one of the decay products in the U-series decay chain.

In the case of samples that contain substantial amounts of detrital components rich in ^{232}Th, the initial ^{230}Th concentration is also expected to be significant, and there is a problem of correcting for this ^{230}Th. Therefore, we consider the samples to be a mixture of two end members: pure carbonate with high ^{230}Th/^{232}Th and a detrital end member with substantial amount of ^{232}Th and initial ^{230}Th. All the dated samples from Misliya are very rich in ^{232}Th, implying that they must have originated with a high concentration of initial ^{230}Th, thus an age correction must be made for the presence of ^{230}Th, ^{238}U and ^{234}U in the detrital component (65). This correction is made using a correction factor, which is the molar ratio of ^{232}Th/^{238}U in the detrital component. In this work, we use a correction factor of 3.8, which is the average crustal value, because Misliya Cave is part of a complex of open prehistoric caves along the western slopes of Mount Carmel, and therefore it is most likely that water was carried into the cave detrital material from various sources.

U-Th results

The dating results are summarized in table S2. All dated samples contain very high detrital material, as evidenced by the very low $^{230}Th/^{232}Th$ ratios ranging between 0.9 to 3.3. Therefore, some caution is warranted in interpreting the ages. The results of the 7 crust samples (one could not be dated) taken from the maxilla yielded (corrected) ages ranging from 19.4±2.5 ky (2σ) to 185 ± 8.0 ky (2σ). Nevertheless, the dates are not randomly distributed along this time-range but rather are grouped: young dates 19-24 ky (2 samples), intermediate dates 45-70 ky (4 samples) and an old date 185.0 ky (1 sample). Similar distribution of dates was obtained for the 11 crust (2 failed to yield results) removed from animal bones and tools: 15-30 ky (6 samples), 50-60 ky (2 samples), >170 ky (2 samples). This may suggest three major growth periods of the crusts in Misliya Cave: 22.7±5.5 ky (n=8); 58.7±7.7 ky (n=6); 178.0±6.0 ky (n=2). Two dates were excluded as they yielded a ± greater than 20ky.

This result suggests that the crust started to build on the Misliya-1 maxilla between 172 to 185 ky ago (or 185 ± 8.0 ky if we use only the data from the maxilla), lending further support to the antiquity of the specimen. The fact that this specimen was found in a distinct archaeological layer, far from the cave wall, excludes the possibility of contamination with host-rock or detrital material, and support the reliability of the older ages. The younger ages most likely represent a later period of the crust growth (yet excluding the possibility of recent intrusion).

How old is Misliya-1?

- All six EMP stratigraphic units in Misliya Cave contain only an Early Levantine Mousterian lithic industry (Tabun D-type). This industry is dated between 250 ky to 140

ky based on radiometric data obtained from Misliya Cave (11), Tabun Cave (13) and Hayonim Cave (12).

- The TL ages of 9 burned flints from the upper part of the EMP archaeological layer from squares close to the location of the fossil (N12, L10), yielded a calculated mean age of 179±48 ky (n=9; 2σ error) (raw data taken from Valladas et al. (11)).

- Direct dating of Misliya-1 provides a U-series age of 70.2±1.6 ky (2σ error) and a combined US-ESR age of 174±20 ky (2σ error). Because (i) Uranium uptake may be quite delayed after death of the organism, and (ii) the difficulty in accurately evaluating the amount of radiation absorbed by the tooth during previous CT-scanning of the specimen, these two ages should be regarded as minimum and maximum possible age for the fossil, respectively.

- The U-Th finite age estimates derived from the calcitic crusts covering fossil remains and flints from the EMP layers at Misliya Cave, range from 243±11/-10 ky to 19±2.5 ky. They suggest a succession of several crystallization events over time. The oldest sample derived from the crust covering the maxilla itself (#6 in table S2) indicates a minimum age of 185±8 ky (2σ error) ago for Misliya-1 (see similar applications in Arsuaga et al. (25), or Daura et al. (66)).

An overview of the dating results using four different methods is displayed in Fig. 2B. The U-series date of 70 ky on the Misliya-1 itself excludes the possibility of recent intrusion. Three methods (combined US-ESR, U-Th, TL) yielded mean dates which coincide (they are in a range from 174 ky to 185 ky). The age range for Misliya-1,

calculated based on the dates directly connected with the fossil (U-Th on crust provides the minimum age and combined US-ESR on the enamel of I^2 the maximum age), is between 177 ky (=U-TH 185 ky-8 ky) and 194 ky (=US-ESR 174 ky+20 ky) (2σ confidence interval, dark band in Fig. 2B). This age range is again well within the age range (250 ky-140 ky) of the EMP sequence in the Levant.

In summary, the remarkable consistency of the dating results deriving from independent methods (carried out in three different independent laboratories) indicates the robustness of the chronological constraints of the Misliya-1 fossil.

Supplementary Text

Comparative analysis of Misliya-1: maxillary morphology

Dental arcade and palate: The dental arcade can be tentatively reconstructed by mirroring the preserved left side. However, points to define the mid-sagittal plane are restricted to the anterior part which leaves a slight degree of uncertainty. Nevertheless, we are confident that the specimen shows a parabolic shape of the dental arch, with the tooth rows diverging posteriorly. Anteriorly, the dental arcade shows an even curvature, contrasting with some Neanderthal specimens which show anterior teeth that are aligned in a rather straight mesiodistal line. The length of the dental arcade (Prosthion to the distal edge of the M^3 alveoli measured along the midline) is 57.0 mm, while the breadth of the dental arcade (M61) is 60.5 mm. Given the slight degree of uncertainty (up to 2mm) that exists for this latter measurement due to the mirroring procedure, the dental arcade breadth may range from 58.5 mm to 62.5 mm. The resulting dental arcade index in Misliya-1 is high (91.2-97.4), falling above the values reported in Neanderthals

(Range=63.5-85.4, n=8) and is within the range of variation in our recent human sample (Range=70.6-99.6, n=31).

Both internal and external alveolar margins progressively diverge from the midline as far posteriorly as M^3. Posterior to M^1, nearly vertical alveolar processes meet the palatine processes abruptly. Anterior to P^4, the palatal surface slopes steeply inferiorly to the alveolar margin throughout the anterior dental region. The palate surface lacks any distinctive features, beside a bony spur opposite M^1 and remnants of the groove for the greater palatine nerve and vessel.

The incisive foramen is placed relatively anteriorly, approximately 7.0 mm posterior to the Orale (the midline point on the hard palate posterior to the central incisor alveoli). This placement in Misliya-1 is more anterior than that reported for specimens attributed to *Homo erectus/ergaster* (ca. 10 mm) (67, 68) and Neanderthals (12 mm) (69, 70) but not as anterior as in *Homo antecessor* (ca. 5 mm) (71). While no data for Pleistocene *H. sapiens* have been published, the value in Misliya-1 is very close to the mean and clearly within the range of our modern human comparative sample (6.8±1.2 mm; range = 4.5-9.1 mm; n = 31).

Zygomatic root: The insertion of the zygomatic root is at the level of the M^1. This is a relatively anterior placement (see the results of the GM analysis in main text) and is similar to the condition reported to characterize recent *H. sapiens*, where the zygomatic process root is located anterior to the M^2 in >95% of cases (72, 73). Neanderthal specimens, in contrast, show a more posteriorly placed zygomatic root (46, 74), either at the M^2 (e.g., Shanidar 2, 4) or at the M^2-M^3 septum (e.g., La Ferrassie 1, La Chapelle-aux-Saints 1, Shanidar 1, 5) (72, 73).

Nasal Floor Morphology: Despite some damage in Misliya-1, the internal nasal floor morphology can be assessed. The nasal floor is clearly not depressed, and appears most consistent with a level configuration (72). Although the anterior nasal margin is not preserved in Misliya-1, it is clear from the surrounding preserved portions that the predominant transverse plane of the posterior portion of the internal nasal floor is placed approximately level with or slightly inferior to the lowermost point of the nasal margin. The preserved nasal floor anterior and lateral to the incisive foramen is smoothly continuous with the posterior nasal floor. Thus, the preserved morphology anteriorly suggests a smooth entrance to the nasal cavity. The lowest preserved point of the internal nasal floor lies lateral to the midline and medial to the lateral wall of the nasal cavity and is located in the posterior 2/3 of the floor. This deepest point of the internal nasal floor is still, however, clearly higher than the lowest point of the inferior floor of the (exposed) maxillary sinus.

A sloped internal nasal floor is considered a less common variant of the more prevalent level internal nasal floor configuration (75). The distinction between these two is not always well-expressed, and depends to some extent on proper orientation of the maxilla in the Frankfort Horizontal plane. These two categories are occasionally combined for specimens in which the exact configuration is difficult to discern (76). Due to the fragmentary state of the Misliya-1 maxilla, it was necessary to estimate the orientation of the specimen relative to the Frankfort Horizontal plane. Thus, while Misliya-1 seems to exhibit a level configuration, a sloped nasal floor cannot be ruled out, and we have conservatively scored the specimen as showing a level/sloped nasal floor configuration. Although variable, this trait characterizes *H. sapiens* (>80%) (75) and is

commonly seen in the Skhul/Qafzeh hominin sample (60%), while it is rare among Neanderthals (20%) who usually show a bi-level configuration (80%). The level/sloped nasal floor configuration may represent the ancestral condition within the genus *Homo* since it is predominant in early and middle Pleistocene fossils from Africa and Europe (75).

Comparative analysis of Misliya-1: dentition

Upper Lateral Incisor: A shallow longitudinal depression is present along the marginal ridges on the lingual surface of the I^2, indicating only very slight shoveling (ASUDAS grade 1). The I^2 lacks a *tuberculum dentale* but a lingual groove is present. The buccal surface shows an enamel fracture on the distal portion of the tooth. Polishing of the edges of the fracture suggests that this occurred during the lifetime of the individual rather than resulted from post-mortem taphonomic factors. Although there is slight damage to the buccal surface, the tooth shows a flat labial face (ASUDAS grade 0/1 based on the plaque for the I^1) and straight incisal edge. The morphological details of the crown suggest a clear departure from the Neanderthal condition, which normally includes marked shoveling, labial convexity and presence of a lingual tubercle (77, 78). Although the specific morphology may differ somewhat from that in Neanderthals, pronounced incisor shoveling is also a well-known feature of *H. erectus* incisors (15, 79) and has also been reported in many Middle and Late Pleistocene Chinese specimens (e.g., Longtan, Panxian Dadong, Jinniushan, Chaoxian, Xujiayao and Huanglong) (80–85). The degree of shoveling and labial curvature also seem slightly greater in the North African Middle Pleistocene specimen from Rabat than in Misliya-1.

Specific comparison of Misliya-1 with the I^2 from Qesem Cave reveals a marked difference in crown morphology, with the Qesem Cave incisor approaching the Neanderthal condition more closely because of its marked shovel shape and labial convexity (21, 78). In sum, the combination of flat labial surface, straight incisal edge, slight shovel shape and lingual groove seen in Misliya-1 are characteristics of *H. sapiens* and are also present in some Pleistocene *H. sapiens* specimens from Qafzeh and Huanglong. Although variation in the mesiodistal (MD) and buccolingual (BL) dimensions of the I^2 do not consistently separate *Homo* taxa, the Neanderthals are characterized by a somewhat expanded BL dimension. The value for the BL diameter in Misliya-1 (7.7 mm) falls below the Zhoukoudian and Neanderthal ranges of variation, but is just encompassed within the variation seen in the Atapuerca (SH) sample (table S5). It is also within the variation of the Qafzeh/Skhul early *H. sapiens* hominins, yet considerably wider compared with recent modern Levantine populations (table S5). Thus, Misliya-1 seems to lack the BL expansion seen in Neanderthals.

Upper Canine: The general shape of the canine is derived (incisor-like), without cingulum or pronounced shoulders. The distal marginal ridge is damaged and a piece of the crown is missing on the disto-lingual aspect. Mesial and distal marginal ridges are present, but the tooth shows only a slight shoveling (ASUDAS grade 1). The lingual surface shows a slight swelling at the base, but there is no *tuberculum dentale*. There is no distal accessory ridge, nor a mesial ridge. The lack of mass-additive traits (14) in the Misliya-1 canine makes it closer to *H. sapiens* than to any other Middle or Late Pleistocene specimen from Africa, Europe or Asia.

The degree of shoveling in Misliya-1 is like that reported for some Middle Paleolithic *H. sapiens* specimens, while Neanderthals uniformly show a more pronounced degree (ASUDAS grade 2+) (78). Specific comparison with the Middle Pleistocene upper canine from Qesem Cave (21) reveals a strong contrast with the Misliya-1 canine. The former shows a much more pronounced degree of shoveling (similar to ASUDAS Grade 6 for the I^1 and Grade 4-5 for the I^2 plaques), *tuberculum dentale* and mesial canine ridge (ASUDAS Grade 2), a constellation of features that is frequently found in Neanderthals and Middle Pleistocene populations from Europe (e.g., Atapuerca-SH) and some Asian specimens (e.g. Xujiayao) (83). The combination of features in Misliya-1 is closer to recent humans (19) and Late Pleistocene *H. sapiens* fossils from Daoxian (82), Qafzeh, and Huanglong.

The MD (8.1 mm) and BL (9.0 mm) dimensions of the Misliya-1 canine are modest compared with the Qesem Cave, Rabat and Middle Pleistocene European specimens but are closer to the mean values in fossil *H. sapiens* samples and larger compared to recent Levantine populations (table S5). The measured crown area (MCA) in the Misliya-1 canine (54.4 mm^2) falls below the values for Rabat (72.2 mm^2) and Qesem (65.5 mm^2) but is close to the mean for the Qafzeh sample (mean ± s.d. = 56.4 ± 7.0 mm^2; range = 48.6–63.0 mm^2; n = 4). Although data for Neanderthals are not generally available in the literature, the upper canine MCA in the late Middle Pleistocene specimen from Bolomor Cave in Spain is larger (64.6 mm^2) than in Misliya-1 (86).

Upper Third and Fourth Premolars: The P^3 shows a single main cusp on both the buccal and lingual sides. A wear facet has resulted in slight dentine exposure on the buccal cusp. The lingual cusp is distinctly smaller and lower than the buccal one. The

distolingual face of the crown is somewhat reduced and the lingual cusp is located more mesially than the buccal cusp (particularly viewed on the enamel-dentine junction (Fig. 2). The essential crest of the lingual cusp presents a small bifurcation, and no accessory cusps or accessory ridges are present. The central furrow is fairly U-shaped and continuous, with only minor accessory grooves. No transverse crest is present. The angle of inclination of the occlusal part of the buccal surface is low relative to the vertical axis of the tooth, resembling *H. sapiens* P^3 (87).

The P^4 crown morphology resembles that of the P^3 in many details. The Misliya-1 P^4 shows a single main cusp on both the buccal and lingual sides of the crown, with the lingual cusp located more mesially than the buccal cusp. The lingual cusp is slightly smaller than the buccal, the mesial and distal crown margins are approximately parallel. The essential crest of the lingual cusp is bifurcated but there are no accessory cusps or mesial or distal accessory ridges present. The central furrow is U-shaped and continuous, with minor accessory grooves. Overall, both premolars show rather simplified crown morphology and resemble recent *H. sapiens* in the absence of accessory tubercles and ridges, and the lack of cingulum and/or buccal grooves.

The expression of discrete morphological traits is not particularly discriminative among Middle/Late Pleistocene *Homo*, but *H. sapiens* are generally characterized by simple occlusal morphologies and low frequencies (or lack) of mesial and distal accessory ridges, accessory marginal tubercles, transverse crests and buccal cingula and/or grooves (14, 77, 78). The Qesem P^3 also shows a relatively simplified occlusal morphology, lacking a continuous crest joining the buccal and lingual cusps (88), and less lingual cusp reduction than in Misliya-1. The occlusal surface of the North African

Middle Pleistocene specimen from Rabat is complicated by the expression of a mesial accessory cusp (P^3) and a mesial accessory ridge (P^4). These traits are also more frequent in Neanderthals, and the Middle Pleistocene populations from Europe and Asia (14), where continuous transverse crests are also more frequent. Although the discrete traits may overlap in their expression, the GM analysis captures the diagnostic differences between Misliya-1 premolars and Neanderthals. Like in *H. sapiens*, Misliya-1 premolars display tall crowns and relatively expanded occlusal polygons. This morphology is even more distinct in Misliya-1 than in the Qafzeh specimens, which show a broader overlap with Neanderthals despite their attribution to *H. sapiens.*

The MD and BL crown diameters in the Misliya-1 upper premolars are modest (table S5) . In particular, the BL dimensions in both teeth fall well below the means in all the fossil comparative samples and outside the Zhoukoudian and Atapuerca (SH) ranges of variation, but within the range of modern Levantine populations (table S5). The total crown base area for the Misliya P^3 (51.6 mm^2) and P^4 (49.7 mm^2) are also modest when compared with Pleistocene *Homo* specimens (e.g., P^4: Rabat = 65.7 mm^2; Cova Negra = 55.8 mm^2). In particular, the values in Misliya-1 fall below the lower limit of the range of variation in the Qafzeh/Skhul sample (P^3: 55.7 - 68.6 mm^2, n = 5; P^4: 50.9 - 61.1 mm^2, n = 4), but Misliya-1 is within the range of P^4 variation in recent humans (53.9 ± 6.2 mm^2) (89).

Upper First Molar: The M^1 in Misliya-1 shows four main cusps, with a large protocone and a small hypocone (ASUDAS grade 2). A small cusp 5 (metaconule) (ASUDAS grade 3) is also present, although wear of the enamel surface has obscured this feature somewhat. No Carabelli's trait is found. The Misliya-1 M^1 departs from the

Neanderthal condition by not showing the skewed rhomboidal crown outline and large and protruding hypocone that characterizes this clade (see 2D GM results). It is also different from the Middle Pleistocene populations from Asia, which are characterized by BL elongated mesial cusps and larger hypocones (e.g., Xujiayao, Hexian and Chaoxian) (83, 84). The Misliya-1 M^1 is more *H. sapiens*-like than Qafzeh in the degree of hypocone reduction and the pattern of cusp size (see below). The small size of the hypocone in Misliya-1 is notable. Hypocone reduction is defined by an ASUDAS score of 2 or below (41). Thus, the hypocone size in Misliya-1 is reduced and the relative size of the hypocone is smaller than the Qafzeh sample, but approaches the values found in Daoxian and Upper Paleolithic *H. sapiens* specimens from Europe (Table S4).

The total crown base area in Misliya-1 (109.2 mm^2) is smaller than Rabat but similar to the mean values in most of the other fossil comparative samples (table S4). Only the Upper Paleolithic and recent *H. sapiens* teeth show considerably smaller crowns.

Cusp proportions and occlusal polygon area of the M^1: The relative sizes of the cusps in the Misliya-1 M^1 show the following order from largest to smallest: protocone, paracone, metacone, hypocone (table S4). Neanderthals are argued to show a derived combination of a much reduced metacone and large hypocone (16), and this same derived condition has recently been found to characterize the Early Pleistocene M^1s from the European site of Gran Dolina as well (90). The Middle Pleistocene East Asian specimen from Chaoxian shows four main cusps which are all nearly equal in size. The Misliya-1 M^1 departs from the Neanderthal pattern by showing a much reduced hypocone (table S4). The hypocone reduction in Misliya-1 is even more pronounced than in the

Pleistocene *H. sapiens* samples from Qafzeh or Daoxian (table S4), and its morphological affinities with *H. sapiens* are clearly expressed.

The relative size of the occlusal polygon joining the cusp tips is reduced in Neanderthals, suggesting a relatively internal placement of the cusp tips on the M^1. The relative occlusal polygon area in Misliya-1 (31.1) falls outside the Neanderthal range of variation (table S4). The value in Misliya-1 is, however, encompassed within the *H. sapiens* range of variation and is also similar to the values reported for African and Asian specimens attributed to *H. erectus/H. ergaster* (16). The angles formed by the sides of the occlusal polygon joining the cusp tips have also been shown to vary taxonomically, with Neanderthals being distinguished by a high (open) angle centered on the metacone (Angle C) (16, 91). The value for this angle in Misliya-1 (107º) falls closest to the mean values seen in fossil and recent *H. sapiens*, but is well above and below the means reported for specimens attributed to *H. erectus/H. ergaster* (96.8 degree) and the Neanderthals (120.9 degree), respectively (16). Thus, overall, the cusp proportions and relative size of the occlusal polygon in Misliya-1 all suggest its closest affinities lie with fossil and recent *H. sapiens*.

Upper Second Molar: The M^2 shows only three main cusps and the hypocone is very small at both the outer enamel surface and the EDJ (ASUDAS grade 1) (Fig. 2). As in the M^1, a small cusp 5 (metaconule) (ASUDAS grade 2) again appears to be present, but there are neither mesial accessory cusps nor any expression of a Carabelli's trait. The presence of cusp 5 in the M^2 does not discriminate Neanderthals and *H. sapiens* samples. Both the M^2s from Xujiayao and Chaoxian show accessory cusps and a well-developed Carabelli's trait. An ASUDAS grade of 0/1 for the hypocone (= hypocone "absence") is

found in similar frequencies in fossil (8.3%) and recent (14%) *H. sapiens*, and Neanderthals (10%) (17). The M^2s from Rabat, Jebel Irhoud (2), Qafzeh/Skhul as well as the North African Aterian specimens from Dar es-Soltan and Grotte de Contrebandiers also show well-developed hypocones (92). While a hypocone is missing in nearly 33% of the M^2s in the Atapuerca (SH) sample (17), these teeth can still be clearly differentiated from *H. sapiens* in their crown shape (see below and GM analysis).

The BL dimension in the Misliya-1 M^2 is similar to those in the comparative samples including modern human populations (table S5), and extreme reduction of the hypocone is responsible for the MD shortening. Total crown base area in Misliya-1 (103.5 mm^2) is smaller than in Rabat (124.2 mm^2) and falls within the range of variation in the Qafzeh sample (mean = 98.5 mm; range = 79.7-112.1 mm; n = 3), as well as that of recent *H. sapiens* males (99.1 ± 11.7 mm^2) and females (92.9 ± 10.4 mm^2) (93).

In addition, the GM analysis of the EDJ shows that the Misliya-1 M^2 falls within the range of variation of *H. sapiens* and does not overlap with the Neanderthal distribution. The latter are characterized by a relatively larger hypocone and the relative distal displacement of the lingual cusps. Even in the case of the Atapuerca (SH) specimens and their strongly reduced hypocones, they fall far from the Misliya-1 specimen because of their characteristic Neanderthal shape.

Upper Third Molar: The M^3 shows only three main cusps, like the M^2, and the hypocone is absent (ASUDAS grade 0). The Misliya-1 M^3 is reduced in size and lacks mesial accessory cusps but features a small cusp 5 (ASUDAS grade 3) along the distal margin of the tooth which is also visible on the EDJ (Fig. 2). There is no expression of a Carabelli's trait. The Qesem M^3 also lacks a distinct hypocone, but does show a cusp 5

(ASUDAS grade 3) along the distal margin of the tooth (21). Morphologically, the M^3 is the most variable of the molars and the expression of crown traits is variable across taxa. As with the M^2, the BL dimension in the Misliya M^3 is similar to those in the comparative samples (table S5), and the loss of the hypocone seems to have mainly affected the MD dimension. The relative sizes of the cusps in the Misliya-1 M^3 show the following order from largest to smallest: protocone, paracone and metacone. Total crown base area in Misliya-1 (78.4 mm^2) falls within the range of variation in recent *H. sapiens* males (84.9 ± 8.9 mm^2) and females (81.1 ± 12.6 mm^2) (86), but is larger than the Qafzeh 3 (72.1 mm^2) and Qafzeh 11 (71.4mm^2) individuals.

Tooth root shape and size: The root of the lateral incisor is convex and tapers almost evenly throughout the root toward the blunt apex, becoming narrower toward the palatal side. The mesial and distal root surfaces manifest a slight longitudinal depression (fig. S4). The labial surface of the canine root is convex, with a slight bending towards the palatal. The root is long, slender and conical. The apical third is narrow mesiodistally and the apex is pointed. A slight vertical longitudinal depression can be noticed on the distal surface (fig. S4). The mild vertical convexity of the buccal aspect of the root and a lingual narrowing of the single root canal as it approaches the apex tend to align the specimen with *H. sapiens* (87). The tip is slightly bent distally. A clear depression along the mesial surface (starting at the middle third) and a weak depression on the distal side are evident. Obvious crown concavity on the mesial surface is noticed, which continues onto the root as a depression (fig. S4). The P^4 also manifests a single root, albeit longer than the P^3. The apical end of the root bends distally. Slight longitudinal depressions are

noticed on both sides of the root. Unlike the P^3, the deeper mid-root depression is noticed on the distal, but not the mesial, aspect of the root.

The M^1 has three long roots that are nearly of the same length (the mesiobuccal root is the longest amongst the three roots). The roots converge into a broad cervical root trunk. The palatal root is curved when seen from mesial and distal views. There is a longitudinal depression on the inner (distal) aspect of the mesiobuccal root. A wide bucco-palatal spread of the mesiobuccal and the distobuccal roots is also noticed, especially of the mesiobuccal root. In the M^2, the palatal root is fused with the mesiobuccal and the distobuccal roots to form a cone-shaped structure. Taurodontism (an enlarged pulp chamber), a common feature in Neanderthals, is absent in the Misliya-1 upper molars (fig. S4).

As roots of the anterior teeth are known to taxonomically distinguish Neanderthals from recent modern humans (44, 94), we compared the Misliya-1 I^2 and C^1 root lengths with those of Neanderthals and early and recent *H. sapiens* (fig. S4). The length of the tooth root in the Misliya-1 I^2 (15.3 mm) is short compared with Neanderthals (17.6 ± 1.9 mm, n = 18) and the Zhoukoudian sample (18.3 mm, n = 2), but longer than in recent humans (13.0 mm ± 1.4 mm, n = 22) (15, 44). The tooth root of the canine is again short (18.3 mm) compared with Neanderthals (22.5 ± 2.5 mm, n = 12) and the Zhoukoudian sample (22.6 ± 0.6 mm, n = 4), but falls just above the range of variation in a recent human sample (16.1 ± 1.4 mm, n = 12) (fig. S4) (15, 44).

<u>The archaeological context of the Misliya-1 hominin</u>

Misliya Cave is located on the western slope of Mount Carmel, at an elevation of ca. 90m, 12km south of the modern city of Haifa (fig. S1). The site is part of a series of

prehistoric caves situated along the western slopes of Mount Carmel. Seven km to the south is Nahal Me'arot (Wadi el-Mughara) with the caves of Tabun, Jamal, el-Wad and Skhul (95–99), while further south is the cave of Kebara (100).

Today the site appears as a rock shelter or an overhang (fig. S1) carved into the cliff of the mountain, composed of a Cretaceous rudist reef. Strongly cemented archaeological sediments (breccias) are found on three terrace-like surfaces at the base of the cliff, all sloping gently to the west. Late Lower Paleolithic remains (Acheulo-Yabrudian) were unearthed on the Lower Terrace (101–103), while Early Middle Paleolithic (EMP) layers are widely exposed on the Upper Terrace, of which an area of ca. 25 m^2 was excavated (Fig. 1A and B; fig. S1) (10, 29, 104). In the eastern part of the Upper Terrace, cemented layers change laterally into softer sediments (hence the soft sediments area "SSA" in Fig. 1B) which are more amenable to excavation and where lithics and animal bones can be extracted without the risk of being broken in the process. This area, where a series of well-preserved Middle Paleolithic hearths and abundant lithics and animal bones were unearthed, was the main focus of our excavation. Lying above the natural bedrock, the archaeological layers are quite thin in this area (ca. 1-1.5 m) apart from the northern (squares I9-I10) and western (e.g., square L15) parts of the excavation where the layers are thicker, ca. 3.5-4m (Fig. 1) (104).

The repeated construction of hearths, the rich faunal assemblages (105) and the high density of the finds (between 2,000 to 3,000 lithic artefacts larger than 2.5 cm per cubic meter) suggest intensive occupation at the site. The largest hearth excavated so far is about a meter in diameter and 20 cm in thickness, and exhibits an alternation of beds cemented by calcareous ash with calcite-free soft carbonaceous microlaminae. Burned

flints, bones and botanical material found in large quantities attest to the habitual use of fire at the site. The site also provided the earliest evidence for vegetal bedding (104). Plant exploitation is also attested by use-wear analysis of the lithics (106).

To date, ca. 50,000 EMP flint artefacts have been studied and no significant change in material culture along the archaeological sequence was observed (10). The Early Levantine Mousterian/Tabun D-type industry is technologically diversified and contains abundant evidence for laminar production along with use of Levallois methods. Levallois reduction involves mostly a unidirectional convergent method for preparation of points and triangular flakes. The tool-kit is dominated by various types of points and retouched blades, the closest analogies of which are the Early Levantine Mousterian industries in Hayonim Cave Layer E and Hummal (10).

Though collapsed, the shape of the site, together with the remnants of enclosing walls, the presence of ancient flowstones and the numerous boulders within the lithified layers and along the slope, suggest that when inhabited, the cave was large. A detailed geo-archaeological study (104) indicates that the last roof collapse occurred at the end of the EMP habitation of the site, after which the cave was abandoned. This is amply indicated by the exposure of EMP layers directly on the surface of the Upper Terrace and by the fact that no evidence for other technological entities was found at the site.

The Misliya Cave faunal assemblage is overwhelmingly dominated by ungulate taxa, with Mesopotamian fallow deer (*Dama mesopotamica*) and mountain gazelle (*Gazella gazella*) being the most common prey species (105). Body-part analysis, age profiles and bone-surface modifications observed in this almost exclusively anthropogenic assemblage all attest to systematic ungulate hunting, carcass transport and

butchery. Hunting was performed using sophisticated gear, employing a large variety of points of different forms and sizes (107).

The EMP layers on the Upper Terrace are divided into six stratigraphic units from the top of the sequence to the bottom (Fig. 1C): Unit 1 - Cemented sediment (breccia); Unit 2 -Terra-rossa soil intrusion; Unit 3 - Heterogeneous, cemented calcareous sediment; Unit 4 - Soft homogeneous compacted sediment; Unit 5 - Homogeneous grayish-brown cemented sediment, which grades laterally (eastward) to the soft sediment of Unit 6; Unit 6 – Relatively soft grayish-brown sediment with numerous indurated patches, containing a series of well-defined hearths (11).

The Misliya-1 maxilla was retrieved from the upper part of Unit 6, in Square N9 (Fig. 1A and B). In this area, the uppermost stratigraphic Units 1-3 were heavily eroded and Unit 4 is only a few cm thick.

Enclosed is a summary of our major arguments against the possibility of Misliya-1 being a recent intrusion:

1. Misliya-1 maxilla was found within undisturbed EMP sediments.
2. The cave roof collapsed during the EMP period, making it unsuitable for human occupation.

3. There is no evidence of post-EMP use of the cave during prehistoric times. No ceramic sherds or other intrusive elements were found in the upper part of unit 6 (where the maxilla was found).

4. The maxilla is covered with the same calcitic crusts as the surrounding EMP bones and artifacts. Such crusts would not have developed on the surface of the maxilla if it was a recent intrusion.

5. The maxilla itself and the crust that covers it were both dated by radiometric dating methods. The dating confirms the antiquity of the bone. The Uranium Series date on dentine of ca. 70 ky is the minimum age of the maxilla and indicates it cannot be a recent intrusion. The combined US-ESR date of the maxilla, in combination with results from other methods (TL, U-series on calcitic crusts), clearly place it within the EMP chronological framework.

Acknowledgements

Misliya Cave is located in the Mount Carmel Nature Reserve, managed by the Israel Nature and Parks Authority. Field work in Misliya Cave was supported by the Dan David Foundation, the Irene Levi-Sala CARE Archaeological Foundation, the Leakey Foundation, the Thyssen Foundation, and the Faculty of Humanities of the University of Haifa. Laboratory work and dating were supported by the Israel Science Foundation (grant no. 1104/12). The anthropological study was supported by the Dan David Foundation, Ministerio de Economía y Competitividad of Spain (MINECO: CGL2015-65387-C3-3-P), Fundación Atapuerca, and The Leakey Foundation. The ESR dating study received funding from the People Programme (Marie Curie Actions) of the European Union's Seventh Framework Programme (FP7/2007-2013) under REA Grant Agreement nº PIOF-GA-2013-626474 and the Australian Research Council Future Fellowship (FT150100215). N.M. is grateful to LaScArBx ANR-10-LABX-52 for support. Work on the virtual specimens was supported by the Life Science Faculty University of Vienna, Oesterreichische Nationalbank, Anniversary Fund, project number 16121, the Swiss National Science Foundation grants No 31003A_156299/1 and 31003A_176319, A.E.R.S. Dental Medicine Organisations GmbH, Vienna, Austria project number FA547014, and the Siegfried Ludwig - Rudolf Slavicek Foundation, Vienna, Austria, project number FA547016.

We thank the following individuals and institutions for providing access to original specimens or scanning of the fossils: D. Carvalho (Museo Nacional de Historia Natural), H. de Lumley (Institut de Paléontologie Humaine), O. Kullmer (Senckenberg Institute Frankfurt), D. Lieberman (Harvard University), A. L. Santos (Museu

Antropológico, Universidade de Coimbra) and P. Mennecier (Musée de l'Homme Paris), G. Koufos (Aristotle University of Thessaloniki), J. Radovcic (Croatian Natural History Museum), A. Froment and A. Balzeau (Muséum National d'Histoire Naturelle), F. Spoor (University College London and MPI Leipzig) and E. Mbua (National Museums of Kenya), C. Stringer and R. Kruszynski (Natural History Museum London), B. Viola (University of Toronto), P. Wrinn, A. Krivoshapkin, and A. Derevianko (Russian Academy of Science), R. Ziegler (Staatliches Museum für Naturkunde Stuttgart), C. Zollikofer and M Ponce de Leon (Zurich University), G. Gruber (Medical University Vienna), M. Teschler-Nicola and E. Winter (Natural History Museum Vienna). K. Matiasek provided background information on the collections from the Dept. of Anthropology, University of Vienna. Shara Bailey provided some comparative data on M^1 cusp areas. We thank M. Dockner for support during μCT scanning, R. Ginner for taking photographs, L. Buchegger and D. Teplanova for segmentation of individual modern human teeth, and F.L. Bookstein for help with the QDA. Preliminary CT scanning was carried out in collaboration with the Laboratorio de la Evolución Humana at the Universidad de Burgos (Spain) with funding provided by the Junta de Castilla y León Project No. BU005A09. R. Quam received financial support from the American Museum of Natural History (USA). L. Rodríguez and R. García received financial support from the Fundación Atapuerca (Spain). A portion of this research was supported by the Ministerio de Ciencia e Innovación and Ministerio de Economía y Competitividad of the Government of Spain, Project Nos. CGL2009-12703-C03-03, CGL2012-38434-C03-01 and CGL2015-65387-C3-2-P (MINECO/FEDER). Israel Antiquities Authority permits numbers for the Misliya Cave excavations are G-16/2001, G-39/2002, G-

14/2003, G-29/2004, G-12/2005, G-12/2006, G-4/2007, G-54/2008, G-52/2009, and G-50/2010.

We wish to thank all the students and volunteers who participated in the cave excavations from the Department of Archaeology, University of Haifa, Israel; the Dan David Laboratory for the Search and Study of Modern Humans, Tel Aviv University, Israel; the Departments of Archaeology; Wroclaw University and Jagiellonian University, Krakow, Poland. Thanks are also due to the Hof-HaCarmel regional council and the Israel Nature and Parks Authority for their assistance and help throughout the years and to A. Behar (Tel Aviv University) for her drawings.

Special thanks are due to the late Dan David and his son, Ariel David, for their inspiration and financial support throughout the years. Thanks also go to O. Bar-Yosef (Harvard University) and A.M. Tillier (University of Bordeaux) who read and commented on a previous version of this paper.

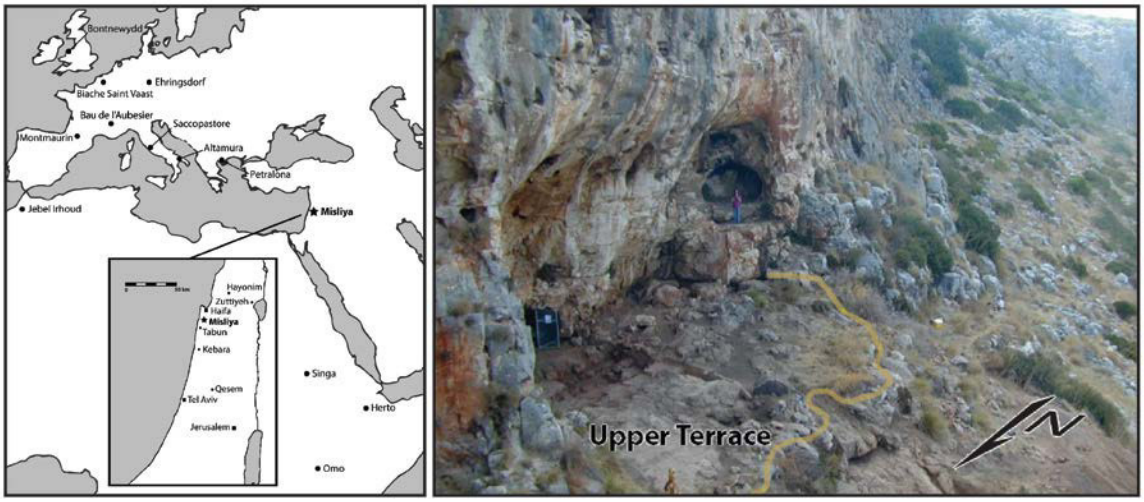

Fig. S1

The geographical location of Misliya Cave, Israel and the excavation areas on the Upper Terrace of the cave. **Left**: Location map with major Early Middle Paleolithic (EMP) sites containing human remains contemporaneous with Misliya-1 (ca. 140-250 ky). Modern cities are symbolized by rectangles. **Right**: The Misliya collapsed cave site at the western cliffs of Mount Carmel. The border of the Upper Terrace (EMP occupation) is marked by a yellow line.

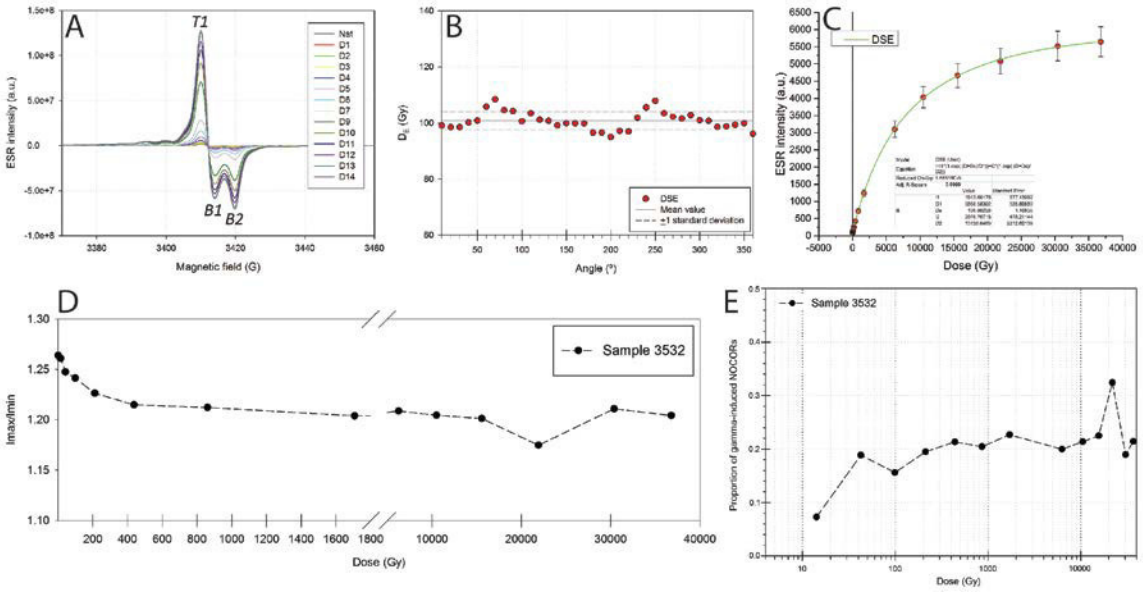

Fig. S2

Electron Spin Resonance (ESR) data collected for the tooth sample #3532 taken from Misliya-1 specimen. (A) Merged ESR spectra over 360º for each dose step. The position of the T1 and B2 peaks used to extract the ESR intensities is indicated; (B) D_E value obtained from the Dose Response Curves (DRC) derived from each angular measurement (every 10º). The solid line represents the mean D_E value; (C) Final DRC based on the mean T1-B2 ESR intensity (error bars are 1 standard deviation) derived from the angular measurements. DSE = double saturating exponential function; (D) Evolution of the I_{max}/I_{min} ratio vs the dose for the sample 3532; (E) Proportion of the additional unstable NOCORs (non-oriented CO_2^- radicals) created by gamma irradiation in comparison with the natural spectrum.

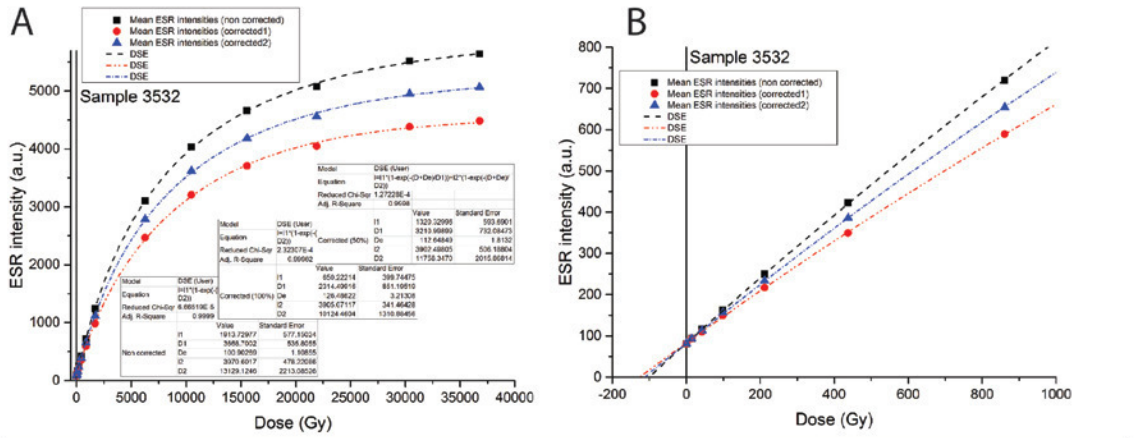

Internal dose rate (µGy/a)	External alpha dose rate	Beta dose rate dentine (µGy/a)	Beta dose rate sediment (µGy/a)	Gamma dose rate + cosmic (µGy/a)	Total dose rate (µGy/a)	Enamel thickness (µm)	Removed surface layer (µm)	D_E (Gy)	p-parameter		US-ESR age (ka)
									enamel	dentine	
18±24	3±2	10±13	90±12	526±24	647±38	907±160	n/a	112.6±1.81	-1*	0.15	174±10

Fig. S3

Direct Combined U-series/Electron Spin Resonance (ESR) dating of the Misliya 1 specimen. (A) Corrected and non-corrected ESR Dose Response Curves (DRCs) obtained for sample #3532 (Misliya 1 lateral incisor). The right graph (B) shows a zoom on the low dose region (<1000 Gy). Key: corrected1= assuming the creation of 100% unstable non-oriented CO2- radicals (NOCORs) by laboratory gamma irradiation; corrected2=creation of 50% of unstable NOCORs. Bottom (table): Combined US-ESR age and dose rate estimates obtained for the tooth sample. Key: (*) because apparent U-leaching is observed in sample #3532 enamel, US-ESR age calculation was performed assuming an Early Uptake in this tissue. This has, however, very little impact on the final age result, as internal dose is less than 3% of the total dose rate (see further details in supplementary text). This combined US-ESR age should be considered as a maximum possible estimate for sample #3532, because of the impossibility to accurately evaluate the laboratory dose given to the tooth sample during the previous CT-scan analyses. In

other words, the true age of the Misliya-1 specimen should be either similar or younger than the calculated Combined US-ESR age estimate (see further details in supplementary text).

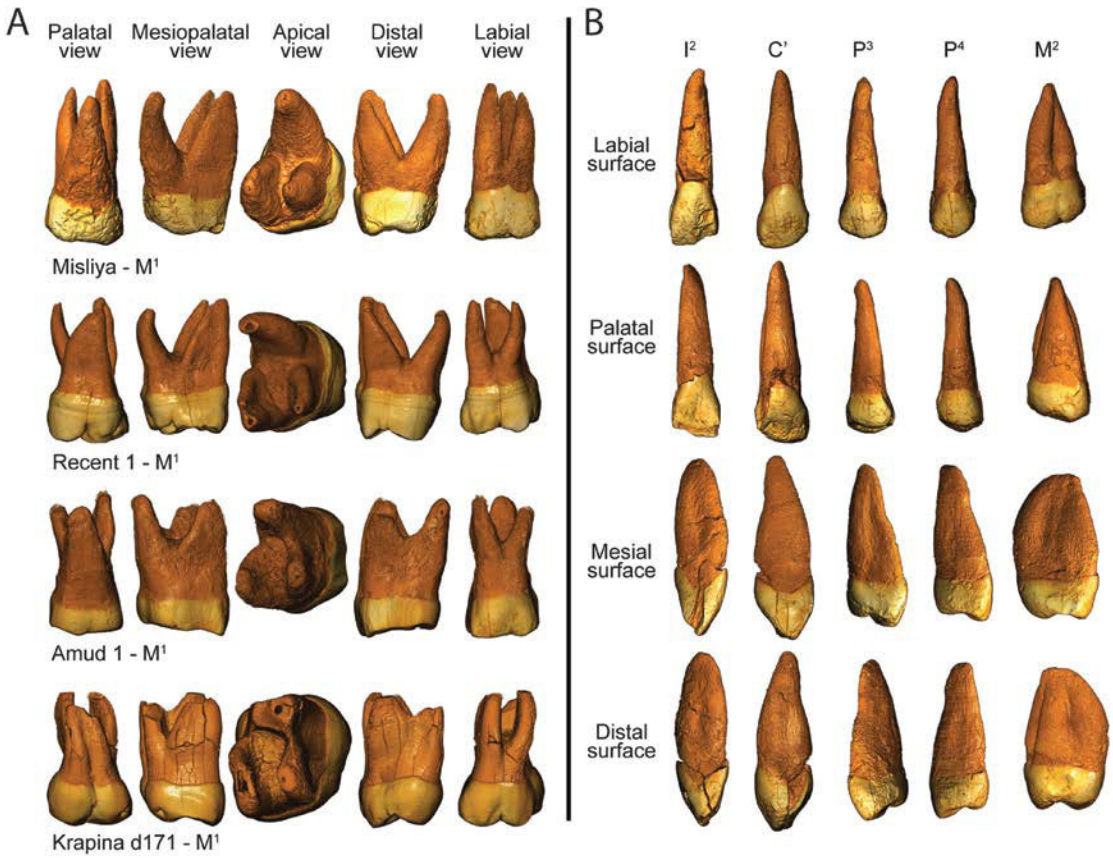

Comparison of roots length (mm) of the lateral incisor and canine

		Early Modern Human mean ± s.d.	Neanderthals mean ± s.d.	Upper Paleolithic mean ± s.d.	Recent mean ± s.d.	Zhoukodian mean ± s.d.
Tooth	Misliya-1	range (n)	range (n)	range (n)	range (n)	range (n)
Upper I²	15.3	15.1 ± 2.9	17.6 ± 1.9	13.7 ± 1.8	13.0 ± 1.4	18.2
		11.7-16.8 (3)	14.7-20.0 (18)	10.8-15.8 (6)	10.1-16.3 (22)	17.3-19.0 (2)
Upper C'	18.3	18.2 ± 2.3	22.5 ± 2.5	16.9 ± 2.1	16.1 ± 1.4	22.5
		15.7-20.0 (3)	17.7-25.2 (12)	12.6-19.6 (8)	13.5-18.7 (12)	21.8 -23.3 (3)

Data for upper I² and C' in Neanderthals and fossil and recent H. sapiens from Le Cabec et al.[44]
Data for upper I² and C' in Zhoukodian from Weidenreich[15]

Fig. S4

Roots shape and size with comparative data: **A:** direct view of the roots of the Misliya-1 M^1 captured from the micro-CT scan, with comparative images of a recent modern human, Amud 1, and Krapina d171; **B:** direct view of the roots of the other Misliya teeth (I^2,C',P^3, P^4, M^2) captured from the micro-CT scan; **C:** comparison of root length (mm) of the lateral incisors and canines.

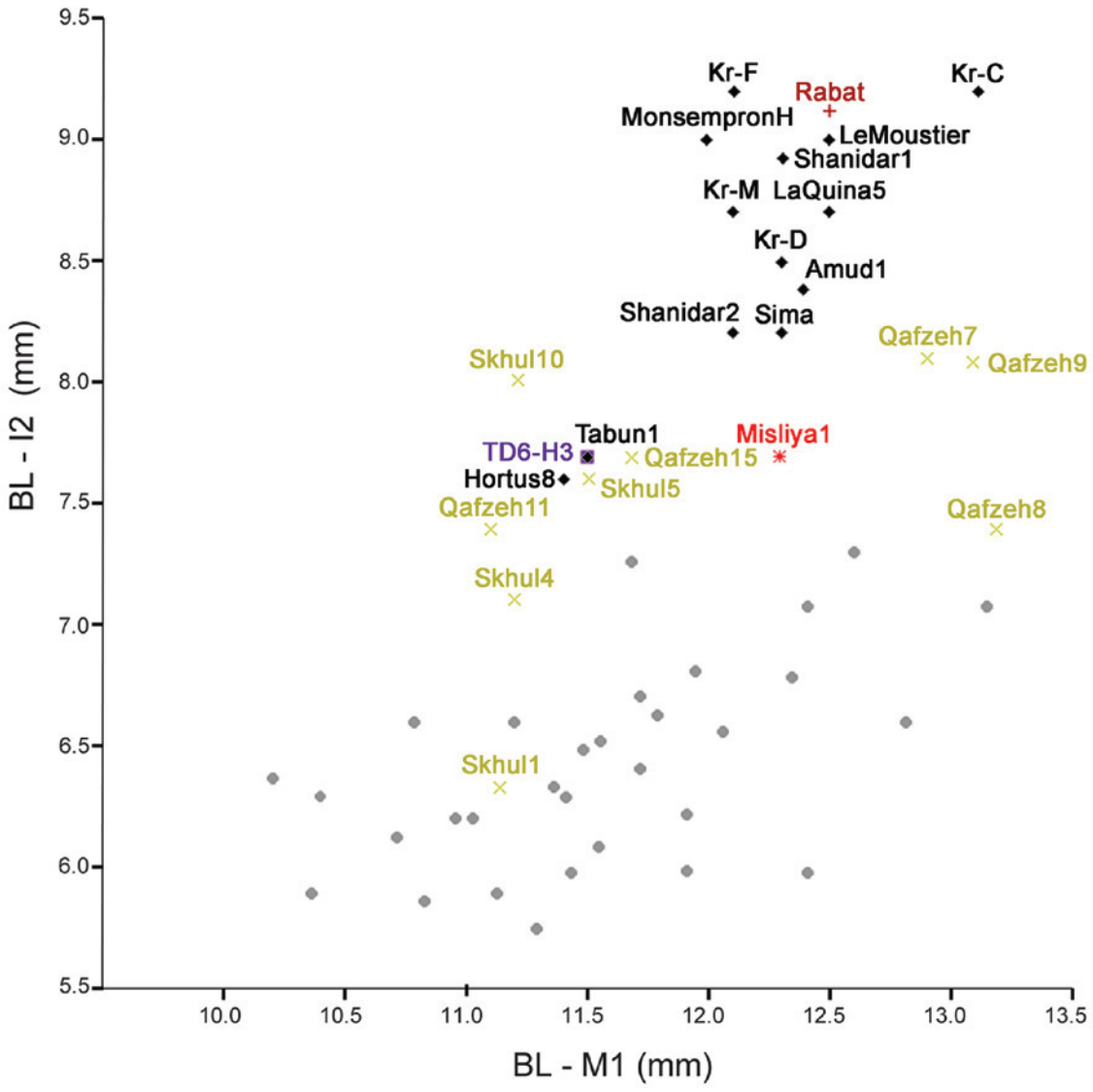

Fig. S5

Ratio of BL dimensions of anterior (I^2) to posterior teeth (M^1). Note the location of Misliya-1 within the range of early modern humans from Skhul and Qafzeh and outside the Neanderthal range.

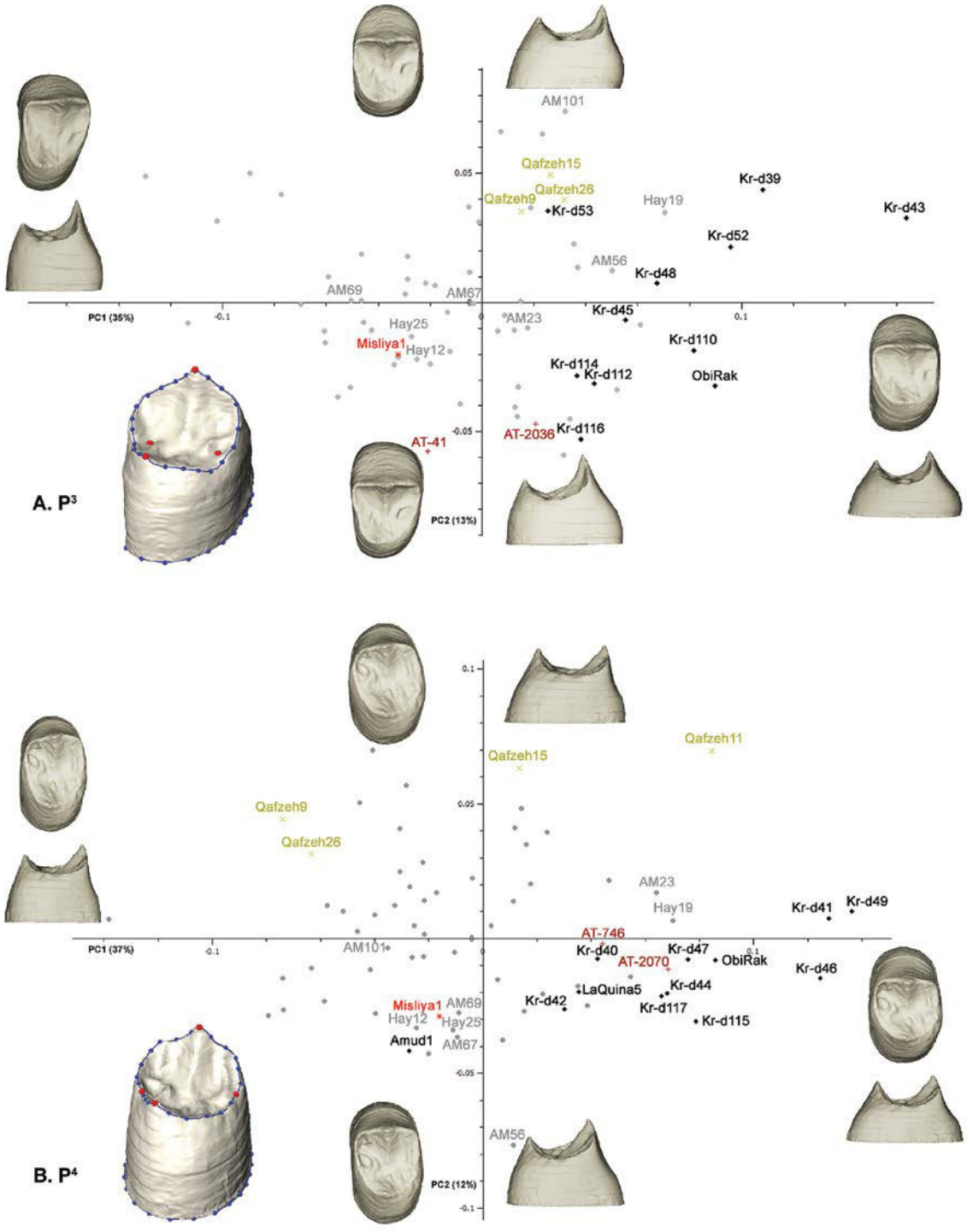

Fig. S6

First two Principal Components (PCs) in shape space and associated warped surfaces at the extremities of the horizontal axes. Shape changes to note in the warpings are; **A:** P^3

and **B:** P^4; PC1 – crown height and width, buccolingual expansion or reduction of the crown base relative to the occlusal rim, lingual tapering of the distal aspect or subequal buccal and lingual aspects. On the left lower side of each of the plots, the landmark configurations used for the respective anatomical unit are represented (landmarks in red, semilandmarks and pseudolandmarks on curves in blue). Abbr.: AT=Atapuerca; Kr=Krapina; AM=Ain-Mallaha (Natufian); Hay=Hayonim Cave (Natufian); Grey dot=Modern human.

Table S1. U-series results on the human bone and tooth from Misliya-1. No age calculations were carried out for U concentrations of ≤ 0.5 ppm or an absolute value of U/Th ≤ 300 but not negative (indicated in italic). Negative U/Th are due to the background being higher than the measurement. All errors are 2-σ.

Sample 3532 (from maxilla MC-Max-H-1)

Spot	U (ppm)	Th (ppb)	U/Th	$^{230}Th/^{238}U$	$^{230}Th/^{238}U$ error	$^{234}U/^{238}U$	$^{234}U/^{238}U$ error	Age (ka)	Age error (ka)
1	***0.2***	411.09	***0***	1.0039	0.084	1.0456	0.0411	n/a	
2	***0***	7.93	***1***	2.9567	1.9578	1.4416	0.2724	n/a	
3	***0***	7.3	***4***	1.1793	0.3545	1.1118	0.1111	n/a	
4	***0.9***	18.57	***51***	0.5093	0.0229	1.1774	0.0168	n/a	
5	1.5	0.03	53743	0.5728	0.0212	1.1666	0.0195	72.3	4.2
6	1.6	-0.13	-11777	0.5915	0.0177	1.1515	0.011	77.2	3.5
7	1.7	0.3	5560	0.5946	0.0241	1.1612	0.0126	76.8	4.7
8	1.8	-0.03	-56346	0.5414	0.0195	1.1913	0.0126	64.9	3.3
9	1.8	0.14	12955	0.5465	0.0191	1.156	0.0153	68.7	3.6
10	2	0	730755	0.5382	0.0165	1.1841	0.0136	65	2.9
11	1.2	0.43	2840	0.5493	0.0228	1.1707	0.0152	67.9	4.1
12	1.2	-0.03	-43328	0.5951	0.0225	1.147	0.0215	78.3	5
13	1.3	-0.18	-6976	0.6148	0.0407	1.1398	0.0231	83	8.8
14	1.4	0.23	6228	0.557	0.0237	1.1753	0.0176	68.8	4.4
15	1.6	0.4	3954	0.5465	0.025	1.1662	0.019	67.8	4.6
16	1.7	0.19	9070	0.5749	0.0222	1.146	0.0219	74.7	4.7
17	1.7	4.11	404	0.5045	0.0166	1.1562	0.0119	61.7	2.9
18	1.5	1.71	873	0.5215	0.0234	1.1578	0.0191	64.3	4.2
19	0.6	9.31	***68***	0.5124	0.0462	1.1195	0.0257	n/a	
20	1.1	12.05	***92***	0.5411	0.0218	1.1626	0.0185	n/a	
21	0.7	7.3	***96***	0.5177	0.0258	1.1289	0.0251	n/a	
22	1	9.3	***105***	0.5841	0.0237	1.1373	0.0188	n/a	
23	0.8	7.23	***112***	0.5505	0.0293	1.1682	0.0176	n/a	
24	1.2	9.82	***125***	0.5725	0.0208	1.1209	0.0144	n/a	
Mean values for each dental tissue									
1-3 Enamel	0.062 ±0.090			1.1054	0.097	1.0709	0.0475	n/a	
5-18 Dentine	1.558 ±0.124			0.5587	0.0088	1.163	0.0059	70.2	1.6

Sample 3533 (from maxilla MC-Max-H-1)

Spot	U (ppm)	Th (ppb)	U/Th	$^{230}Th/^{238}U$	$^{230}Th/^{238}U$ error	$^{234}U/^{238}U$	$^{234}U/^{238}U$ error	Age (ka)	Age error (ka)
1	1.5	22.73	***65***	0.451	0.0188	1.1053	0.0126	n/a	
2	1	29.82	***33***	0.5211	0.0234	1.1333	0.0186	n/a	
3	0.6	76.21	***8***	0.4809	0.0291	1.1067	0.0155	n/a	
4	0.8	43.28	***18***	0.4451	0.0281	1.1427	0.0182	n/a	
5	1.1	18.48	***57***	0.4438	0.0255	1.1523	0.0222	n/a	
6	1	24.74	***41***	0.472	0.0174	1.1304	0.0174	n/a	
7	0.9	43.72	***21***	0.4126	0.0159	1.1021	0.0153	n/a	
8	1.1	28.46	***39***	0.4088	0.0176	1.0915	0.0189	n/a	

Table S2. Detailed dating results of the calcitic crust covering the maxilla, animal bones and lithic artefacts.

No.	Location	^{238}U [ppm]	Error	Uncorrected $^{234}U/^{238}U$	Error	Corrected $^{234}U/^{238}U$	Error	Uncorrected $^{230}Th/^{234}U$	Error	Corrected $^{230}Th/^{234}U$	Error	$^{230}Th/^{232}Th$	Error	Uncorrected age [ky]	2s [ky] +	2s [ky] -	Corrected age (3.8) [ky]
1	Maxilla 1	0.910	0.001	1.12007	0.00241	1.18393	0.00254	0.54913	0.00336	0.34658	0.00212	1.5	0.01	85	0.8	-0.8	46
2	Maxilla 2	0.541	0.001	1.07099	0.00371	0.52541	0.00182	0.83774	0.00497	3.21120	0.01904	0.8	0.00	190	3.4	-3.3	31*
3	Maxilla 3	0.503	0.000	1.08354	0.00265	1.40571	0.00344	0.77633	0.00530	0.16269	0.00111	0.9	0.01	157	2.5	-2.5	19
4	Maxilla 4	0.648	0.001	1.09884	0.00144	1.30700	0.00171	0.80214	0.00233	0.48330	0.00141	1.1	0.00	168	1.2	-1.2	70
5	Maxilla 5	0.667	0.001	1.08507	0.00207	1.27354	0.00243	0.69623	0.00381	0.16776	0.00092	0.9	0.00	126	1.4	-1.3	24
6	Maxilla 6	0.535	0.000	1.10364	0.00275	0.85558	0.00213	1.11889	0.00553	0.78630	0.00389	0.6	0.00	equilibrium	8.0	-8.0	185
7	Maxilla 7	0.927	0.001	1.11644	0.00279	1.15567	0.00289	0.55097	0.00224	0.42009	0.00170	2.0	0.01	86	0.6	-0.5	58
8	Maxilla 8	2.108	0.001	1.12369	0.00209	1.13125	0.00210	0.46343	0.00188	0.43443	0.00176	7.5	0.03	67	0.4	-0.4	61
9	Sq=K11b; Ht=145-150	0.314	0.000	1.06803	0.00274	1.26243	0.00323	0.94751	0.00490	0.82871	0.00428	1.1	0.01	288	8.3	-7.7	172
10	Sq=K11b; Ht=100-105 (f)	1.509	0.001	1.07497	0.00104	1.09876	0.00106	0.40153	0.00150	0.22867	0.00086	1.5	0.01	55	0.3	-0.3	28
11	Sq=N9b; Ht=121-127 (b)	0.731	0.001	1.04914	0.00178	1.18007	0.00200	0.97876	0.00330	0.93079	0.00314	1.2	0.00	359	11.0	-10.0	243
12	Sq=N9b; Ht=105-108 (b)	1.239	0.001	1.03640	0.00238	1.06763	0.00245	0.54299	0.00275	0.17566	0.00089	1.0	0.01	85	0.7	-0.7	21
13	Sq=N9b; Ht=82-86 (b)	3.158	0.004	1.06636	0.00173	1.07787	0.00175	0.35581	0.00111	0.25210	0.00079	2.1	0.01	48	0.2	-0.2	31
14	Sq=N9b; Ht=108-113 (b)	0.844	0.001	1.03684	0.00191	1.08112	0.00199	0.61349	0.00446	0.18378	0.00134	1.0	0.01	103	1.3	-1.3	22
15	Sq=L9b; Ht=128-133 (b)	0.585	0.001	1.04423	0.00212	1.50656	0.00305	0.95988	0.00915	0.68150	0.00649	0.9	0.01	319	20.6	-17.3	114
16	Sq=N9b; Ht=113-118 (b)	1.014	0.001	1.02545	0.00221	1.07250	0.00231	0.70272	0.00261	0.19020	0.00071	0.9	0.00	131	1.0	-1.0	23
17	Sq=L9b; Ht=105-116 (b)	1.183	0.001	1.02925	0.00119	1.05783	0.00123	0.54429	0.00287	0.12337	0.00065	0.9	0.01	85	0.7	-0.7	14
18	Sq=M9b; Ht=108-115 (b)	0.872	0.001	1.03070	0.00188	1.10744	0.00202	0.82326	0.00375	0.42430	0.00193	1.0	0.00	185	2.4	-2.4	59
19	Sq=K11b; Ht=185-190 (b)	3.188	0.003	1.02253	0.00163	1.03314	0.00165	0.59819	0.00138	0.415089	0.00096	3.3	0.01	99	0.4	-0.4	58
20	Sq=L9 hearth: Ht=155-160	0.600	0.001	1.03006	0.00139	2.17349	0.00294	1.15075	0.00446	3.78927	0.01469	1.0	0.00	equilibrium			equilibrium

Error of ages are reported as 2σ; isotopic ratios are 1σ.

Sq=Square; Ht=Height below datum in cm.

(b)=Crust on bone; (f)=Crust on flint.

*=unreliable date, since $^{230}Th/^{234}U > 3.0$

Table S3. Top: Radioelement concentrations obtained for the raw sediment samples. In italics, mean values with corresponding 1 standard error. These values were used for beta dose rate evaluation. Bottom: ESR fitting results obtained for the four different fitting functions and options. SSE = Single Saturating Exponential Function; DSE = Double Saturating Exponential Function; (*) DE results derived from the corrected ESR intensities assuming 100% of gamma-induced NOCORs; (**) assuming 50% of gamma-induced NOCORs. In bold, the equivalent dose (DE) values used for the final US-ESR age calculation.

Sediment sample	**Layer**	**Corresponding tooth**	**U (ppm)**	±	**Th (ppm)**	±	**K (%)**	±
1	Upper unit 6	Lateral incisor (sample #3532)	1.030	0.078	1.520	0.080	0.540	0.021
2			1.520	0.087	1.620	0.083	0.552	0.022
3			1.830	0.094	1.460	0.078	0.538	0.021
4			1.280	0.082	1.980	0.096	0.624	0.025
Mean			***1.415***	***0.171***	***1.645***	***0.116***	***0.551***	***0.028***

Sample	**Function**	**Adj.R^2**	**D_{max} (Gy)**	**D_E**	**error**	**D_{max}/D_E**
lateral incisor (sample #3532)	SSE	0.9999	861	98.7	1.302	8.7
	DSE	0.9999	36786	100.9	1.109	n/a
	DSE*	0.9996	36786	126.5	3.213	n/a
	DSE**	**0.9998**	**36786**	**112.6**	**1.813**	**n/a**

Table S4. Total crown base area, relative cusp base areas and relative occlusal polygon area in the M1 in Misliya-1 and Pleistocene and recent humans.

Specimen/Sample	Total Crown Base Area (mm^2) Mean ± s.d. range (n)	Relative Protocone Area (%) Mean ± s.d. range (n)	Relative Paracone Area(%) Mean ± s.d. range (n)	Relative Metacone Area (%) Mean ± s.d. range (n)	Relative Hypocone Area (%) Mean ± s.d. range (n)	Relative Polygon Area (%) Mean ± s.d range (n)
Misliya-1	109.2	35.3	27.4	22.8	14.5	31.1
Rabat	122.0	26.2	25.0	19.1	29.7	28.4
Chaoxian 1	131.8	26.6	25.1	24.2	24.1	
H. erectus/H. ergaster	115.5 ± 6.8 105.2-124.1 (5)	29.9 ± 2.2 26.4-31.8 (5)	24.9 ± 2.3 21.8-27.7 (5)	22.9 ± 1.7 21.3-25.7 (5)	22.3 ± 0.4 21.8-23.0 (5)	32.9 30.8-35.0 (2)
Atapuerca-SH	106.7 ± 11.9 84.1-129.8 (11)	34.8 ± 2.1 31.8-37.2 (11)	24.8 ± 1.1 23.1-26.5 (11)	22.9 ± 1.8 18.8-24.8 (11)	21.2 ± 1.7 19.8-23.9 (11)	25.2 ± 4.0 21.2-32.3 (10)
Non-SH Mid. Pleist. Europe	115.5 ± 17.0 101.9-134.5 (3)	31.1 ± 3.7 25.9-34.1 (4)	24.8 ± 0.9 23.6-25.7 (4)	20.1 ± 2.6 17.8-23.5 (4)	24.0 ± 1.6 22.3-25.9 (4)	
Neanderthals	112.3 ± 16.6 78.2-153.4 (19)	29.9 ± 2.4 26.0-34.6 (21)	25.8 ± 2.1 22.0-30.6 (21)	20.6 ± 1.8 16.5-24.8 (21)	23.7 ± 2.1 19.0-26.7 (21)	26.7 ± 1.8 23.2-30.5 (17)
Qafzeh	111.3 ± 12.7 95.8-134.5 (7)	31.3 ± 2.3 28.2-34.4 (7)	24.8 ± 1.6 22.8-27.6 (7)	21.3 ± 2.5 16.9-24.6 (7)	22.8 ± 5.0 15.9-29.6 (7)	33.3 ± 2.7 29.6-36.6 (4)
Daoxian	76.3±4.7 71.8-81.2 (3)	32.5 ± 1.0 30.5-33.0 (7)	25.9 ± 1.4 24.0-28.5 (7)	22.3 ± 1.3 20.2-24.2 (7)	20.3 ± 1.3 18.6-21.7 (7)	34.7 ± 1.3 33.2-35.4 (3)
Upper Paleolithic H. sapiens	99.6 ± 10.2 81.7-120.7 (14)	31.8 ± 1.5 29.6-36.2 (15)	25.7 ± 2.3 22.8-31.7 (15)	22.4 ± 1.7 20.0-26.0 (15)	20.1 ± 3.0 14.9-24.8 (15)	32.7 ± 1.9 28.6-33.5 (5)
Recent H. sapiens	96.6 ± 14.0 71.7-138.6 (59)	31.0 ± 2.0 24.9-35.8 (59)	25.8 ± 2.1 21.4-31.9 (59)	22.9 ± 1.8 18.0-26.9 (59)	20.4 ± 2.5 14.8-26.9 (59)	37.5 ± 5.4 27.0-50.4 (24)

Total crown base area is equal to the sum of the individual cusp areas

Relative cusp areas = (Absolute cusp area/total crown base area) x 100

Data for comparative samples (except Chaoxian and Daoxian) from Quam et al. (*39*); Martinón-Torres et al. (*40*)

Data for Chaoxian from Bailey and Liu (*80*)

Data for Daoxian from Liu et al. (*9*)

Relative polygon area = (Absolute polygon area x 100)/Total crown base area

Data for H. erectus/H. ergaster relative polygon area from Bailey (*16*)

Table S5. Mesiodistal (MD) and buccolingual (BL) crown dimensions (mm) of the maxillary teeth of Misliya-1 compared with Pleistocene and recent humans.

	I^2		C^1		P^3		P^4		M^1		M^2		M^3	
Specimen/Sample	**MD mean ± s.d. range (n)**	**BL mean ± s.d. range (n)**	**MD mean ± s.d. range (n)**	**BL mean ± s.d. range (n)**	**MD mean ± s.d. range (n)**	**BL mean ± s.d. range (n)**	**MD mean ± s.d. range (n)**	**BL mean ± s.d. range (n)**	**MD mean ± s.d. range (n)**	**BL mean ± s.d. range (n)**	**MD mean ± s.d. range (n)**	**BL mean ± s.d. range (n)**	**MD mean ± s.d. range (n)**	**BL mean ± s.d. range (n)**
Misliya-1	7.7	7.7	8.1	9.0	7.3	9.4	6.8	9.1	10.4	12.3	9.7	12.3	8.9	11.8
Qesem	7.4	7.6	8.8	9.8	7.8	9.9							9.7	11.1
Rabat	8.2	9.1	9.8	10.5			7.4	11.3	12.4	12.5	11.9	13.1		
BOU VP 16/1 (R)			7.0	9.0							12.0	12.8	8.6	11.9
BOU VP 16/1 (L)			8.0	9.0							11.8	12.8	8.6	11.9
BOU VP 16/5							7.2	9.2						
BOU VP 16/6									12.1	11.8				
BOU VP 16/42							7.8	10.4						
Daoxian			7.8 ± 0.2 7.6-8.0 (3)	8.3 ± 0.4 7.9-8.7 (3)	7.6 ± 0.3 7.3-7.9 (3)	10.1 ± 0.2 9.9-10.2 (3)	6.3 ± 0.2 6.2-6.5 (3)	9.1 ± 0.5 8.5-9.8 (4)	10.4 ± 0.5 9.8-11.0 (12)	11.3 ± 0.4 10.2-11.8 (12)	9.6 ± 0.5 9.0-10.0 (4)	11.4 ± 0.7 10.5-12.0 (4)	8.9 ± 0.6 8.3-9.5 (3)	10.3 ± 0.7 9.7-11.0 (3)
Zhoukoudian	7.7 6.8-8.3 (3)	8.1 8.0-8.2 (3)	9.4 ± 0.7 8.5-10.5 (5)	10.1 ± 0.4 9.8-10.6 (5)	8.4 ± 0.6 7.4-9.2 (6)	11.6 ± 0.8 10.5-12.6 (7)	7.8 ± 0.6 7.0-8.8 (11)	11.4 ± 0.6 10.3-12.5 (11)	11.2 ± 0.9 10.0-13.1 (8)	12.5 ± 0.7 11.7-13.7 (7)	10.5 ± 0.7 10.0-12.2 (8)	12.6 ± 0.5 11.9-13.4 (8)	9.6 ± 0.5 8.7-10.5 (10)	11.5 ± 0.8 10.4-12.5 (10)
Atapuerca (SH)	7.8 ± 0.3 7.2-8.2 (17)	7.8 ± 0.3 7.3-8.3 (18)	8.6 ± 0.4 8.1-9.6 (18)	9.8 ± 0.6 9.0-10.7 (19)	7.9 ± 0.5 7.2-8.9 (14)	10.5 ± 0.6 9.6-11.8 (15)	7.6 ± 0.5 7.0-8.8 (16)	10.4 ± 0.6 9.5-11.5 (16)	11.1 ± 0.7 9.9-12.3 (17)	11.5 ± 0.7 10.3-13.0 (17)	9.9 ± 0.9 8.1-11.6 (18)	12.2 ± 0.8 11.0-13.8 (18)	8.6 ± 0.6 7.4-9.3 (19)	11.5 ± 0.9 10.1-13.0 (19)
Neanderthals	7.8 ± 0.6 6.3-9.0 (15)	8.3 ± 0.5 7.8-9.9 (15)	8.2 ± 0.5 7.4-9.3 (20)	9.5 ± 0.6 8.6-10.6 (21)	7.4 ± 0.6 6.5-8.6 (19)	10.4 ± 0.6 9.0-11.4 (19)	7.1 ± 0.5 6.4-8.2 (20)	9.9 ± 0.6 9.0-11.2 (20)	11.1 ± 0.8 10.0-13.0 (22)	11.9 ± 0.4 11.1-12.5 (22)	10.5 ± 0.8 9.3-12.0 (19)	12.3 ± 1.2 10.0-14.5 (19)	9.6 ± 0.7 8.3-11.0 (16)	12.0 ± 1.0 10.0-14.0 (16)
Qafzeh/Skhul	7.5 ± 0.8 6.2-8.8 (10)	7.4 ± 0.6 6.2-8.1 (11)	8.4 ± 0.5 7.5-9.4 (11)	9.2 ± 0.8 8.0-10.3 (11)	7.8 ± 0.5 7.1-8.7 (8)	10.4 ± 0.4 10.0-11.1 (9)	7.1 ± 0.4 6.5-7.6 (9)	10.2 ± 0.8 8.4-11.0 (10)	11.3 ± 0.6 9.9-12.4 (18)	12.2 ± 0.7 11.2-13.3 (18)	10.5 ± 1.1 8.6-12.2 (10)	12.0 ± 0.7 10.7-13.0 (10)	9.3 ± 0.2 9.0-9.5 (6)	11.7 ± 1.1 10.4-13.5 (6)
Euro. UP H. sapiens	6.6 ± 1.1 5.0-8.3 (9)	7.3 ± 0.9 6.3-9.0 (9)	7.7 ± 0.7 6.0-8.4 (10)	9.4 ± 0.8 7.5-10.4 (10)	6.7 ± 1.1 4.6-7.8 (10)	9.5 ± 0.9 8.0-11.0 (10)	6.6 ± 1.0 5.0-8.0 (10)	9.5 ± 0.9 8.0-11.1 (10)	10.4 ± 0.6 9.4-11.7 (11)	12.0 ± 0.9 11.0-13.5 (11)	10.0 ± 1.0 8.0-11.0 (11)	12.5 ± 1.0 10.9-14.0 (11)	9.7 ± 1.1 8.0-12.0 (9)	11.8 ± 1.7 8.0-13.5 (9)
Recent Humans	6.8 ± 0.5 5.7-7.8 (65)	6.9 ± 0.5 5.8-7.1 (65)	7.8 ± 0.4 6.6-8.2 (20)	8.4 ± 0.6 6.4-9.2 (20)	6.9 ± 0.5 6.4-7.8 (34)	9.2 ± 0.4 7.7-9.9 (34)	6.7 ± 0.4 5.6-7.7 (22)	9.7 ± 0.5 7.8-10.3 (22)	10.4 ± 0.6 9.8-12.5 (112)	11.8 ± 0.6 10.7-12.5 (112)	10.0 ± 0.9 9.2-11.4 (17)	12.1 ± 0.7 10.1-12.8 (17)	9.2 ± 0.6 7.4-10.3 (10)	11.2 ± 0.7 8.9-12.4 (10)

Data for Misliya, Qesem, Rabat, Atapuerca (SH) and recent humans measured by the authors.

Data for Herto specimens from White et al. (*4*)

Data for Daoxian sample from Liu et al. (*9*)

Data for Zhoukoudian and Neandertal samples from Bermudez de Castro (*108*)

Data for Qafzeh/Skhul from McCown & Keith (*109*), Vandermeersch (*110*) and Tillier (*111*)

Data for Euro. UP H. sapiens from Vlćek (*112*), Sládek et al. (*113*) and Trinkaus et al. (*114*)

Recent humans = Bedouin teeth, Israel

Table S6. top) Eigenvalues and percentage of explained variance for the first 10 PCs in shape space for all four examined anatomical units; middle) Likelihood ratios (LRs) from the Quadratic Discriminant Analysis on ranges of principal component scores for the maxilla, P3, P4, and M2. LRs lower than 0.146 (bold) indicate likely affiliation to modern humans. LRs between 0.146 and 6.3 (italic) provide equivocal signals, and LRs above 6.3 indicate likely affiliation to Neanderthals. PC ranges up to 1-5 are reported; bottom) misclassified specimens and equivocal results of the QDA.

Principal Component Analysis (PCA)-Shape Space

	Maxilla		P^3		P^4		M^1 (2D)		M^2	
PC	**Eigenvalue**	**Variance %**	**Eigenvalue**	**Variance %**	**Eigenvalue**	**Variance %**	**Eigenvalue**	**Variance %**	**Eigenvalue**	**Variance %**
1	0.00821	57.15	0,00279	34,68	0,00290	37,38	0,00053	45,45	0,00276	25,80
2	0.00197	13.75	0,00101	12,53	0,00092	11,89	0,00018	15,57	0,00152	14,21
3	0.00087	6.09	0,00088	10,93	0,00069	8,84	0,00013	11,20	0,00113	10,62
4	0.00066	4.57	0,00065	8,11	0,00061	7,90	0,00011	9,09	0,00097	9,07
5	0.00050	3.47	0,00041	5,15	0,00048	6,21	0,00006	4,78	0,00078	7,29
6	0.00042	2.93	0,00041	5,04	0,00044	5,69	0,00003	2,77	0,00051	4,81
7	0.00036	2.51	0,00029	3,64	0,00035	4,56	0,00002	2,03	0,00037	3,44
8	0.00026	1.80	0,00024	3,00	0,00025	3,18	0,00002	1,74	0,00032	3,03
9	0.00022	1.54	0,00018	2,19	0,00020	2,62	0,00002	1,54	0,00029	2,70
10	0.00019	1.34	0,00016	1,99	0,00014	1,77	0,00001	1,15	0,00023	2,17

Table S7. Specimens used for 2D analyses of crown outline (M1), cusp relative area (M1), teeth reduction (BL-I2/M1 index), 3D analyses of the maxilla and CEJ and EDJ in P3, P4 and M2.

	Recent Modern Humans, Upper Paleolithic and Epipaleolithic Modern *Homo*	**Early Modern Humans (EMH)**	**Neanderthals**	**Early and Middle Pleistocene *Homo***
3D Maxilla	Ain Mallaha-23, Bmo-3, Combe Capelle, Dolni Vestonice-3, Liujiang, Mladec-1, Predmosti-3, Ohalo-II-1, Africa (5), Asia (3), Australia (2), Bedouin (2), Europe (3), Papua-NG (2), **(Total n=25)**	Qafzeh 9, Skhul-4, 5, Jebel Irhoud-1, **(Total n=4)**	Amud-1, Saccopastore-1, 2, Saint Cesaire, Shanidar, **(Total n=5)**	Atapuerca-SH5, Arago-21, Kabwe-1, Petralona-1 **(Total n=4)**
3D Upper P^3	Ain Mallaha 23, 56, 67, 69, 101, HaYonim 12, 19, 25, Africa (14), Asia (3), Australia (4), Avar (7), Bedouin (5), Europe (8), Papua-NG (5), **(Total n=54)**	Qafzeh 9, 15, 26, **(Total n=3)**	Krapina d39, d43, d45, d48, d52, d53, d110, d112, d114, d116, Obi-Rakhmat, **(Total n=11)**	Atapuerca AT-41, AT-2036, **(Total n=2)**
3D Upper P^4	Ain Mallaha 23, 56, 67, 69, 101, HaYonim 12, 19, 25, Africa (13), Asia (3), Australia (4), Avar (6), Bedouin (4), Europe (6), Papua-NG (6), **(Total n=50)**	Qafzeh 9, 11, 15, 26, **(Total n=4)**	Amud-1, La Quina-5, Krapina d40, d41, d42, d44, d46, d47, d49, d115, d117, Obi-Rakhmat, **(Total n=12)**	Atapuerca AT-746, AT-2070, **(Total n=2)**
3D Upper M^2	Ain Mallaha 23, 56, 67, 69, 101, HaYonim 12, 19, 25, Liujiang, Africa (15), Asia (3), Australia (5), Avar (7), Bedouin (4), Europe (7), Papua-NG (8), **(Total n=58)**	Qafzeh 9, 11, 15, 26, **(Total n=4)**	Amud-1, Krapina d96, d98, d135, d165, d166, d169, d172, d177 **(Total n=9)**	Atapuerca AT-12, AT-960, **(Total n=2)**
2D Crown Outline M^1	Abri Pataud (1), Abu Gosh-747, Africa (2), Australia (2), Avar (1), Bedouin (9), Dar es-Soltan H9, Early Arab (1), Ain Mallaha (4), Europe (2), Fontechevade (1), HaYonim (2), Laugerie Basse (1), Liujiang (1), Mladec-1, Nahal Oren-BD, Neolithic (2), Netiv HaGdud (1), Papua-NG (2), Parpallo (2), Pekiin (10), San Nicolas (1), South America (2), Tabun (Series II Chimney II), Yiftahel (2), **(Total n=54)**	Qafzeh 4, 5, 6, 7, 9, 10, 11, 15, Skhul 1, Daoxian DX1, DX28, **(Total n=11)**	Cova Negra 42175, Krapina d100, d101, d134, d136, d171, d174, La Ferrassie 8, La Quina-5, Obi-Rakhmat, Petit Puymoyen 2, Mx6, Pinilla del Valle-Camino (1), Tabun 1, **(Total n=14)**	Atapuerca AT-16, 20, 26, 138, 139, 196, 406, 587, 812, 944, 959, 2071, 2076, 3177, 3424, 4317, 5840, 5899, Chaoxian (1), Hexian (1), Steinheim (1), Tubo PA1471, Xujiayao PA1480, Rabat (1), **(Total n=24)**
Relative Cusp Area	Abri Pataud (2), Dolni Vestonice (1), Europe (8), Fontechevade (1), Galeria Cisterna (1), La Madelaine (1), Laugerie-Basse (1), Les Rois (2), Mladec (2), North Africa (6), Northeast Asia (15), Oceania (17), Parpallo (2), St. Germaine la Riviere (2), Tabun (Series III) (1), Vachons (1), West Africa (13), **(Total n=76)**	Qafzeh 4, 5, 6, 9, 10, 11, 15, **(Total n=7)**	Arcy-sur-Cure 39, 45, Cova Negra CN 42175, Krapina d100, d101, d134, d171, A, C, D, Kulna (1), La Ferrassie 8, La Quina 18, Le Moustier (1), Monsempron h, Obi-Rakhmat (1), Petit Puymoyen 2, Pinilla del Valle-Camino (1), Saccopastore 2, St. Cesaire (1), Taddeo (1), **(Total n=21)**	Arago 31, Atapuerca AT-20, 138, 196, 406, 812, 959, 2071, 3177, 3178, 4317, 5804, Chaoxian 1, Gran Dolina ATD6-11, 6-69, 6-103, Petralona (1), Pontnewydd 4, Sangiran 4, 7-3, 7-9, 7-37, Steinheim (1), Zhoukoudian L140, Rabat (1), **(Total n=25)**
Tooth Size Proportions BL - I^2/M^1	Bedouin (19), Ain Mallaha (9), HaYonim (3), **(Total n=31)**	Qafzeh 7, 8, 9, 11, 15, Skhul 1, 4, 5, 10, **(Total n=9)**	Hortus 8, Krapina C, D, F, M, La Quina-5, Le Moustier (1), Monsempron h, Shanidar 1, 2, Tabun 1, **(Total n=11)**	Atapuerca TD6, AT-20, Rabat (1), **(Total n=3)**

(n) = number of specimens used for a given analysis

As we also used isolated teeth for the current analyses, many sites lack individual number

References and Notes

1. J.-J. Hublin, A. Ben-Ncer, S. E. Bailey, S. E. Freidline, S. Neubauer, M. M. Skinner, I. Bergmann, A. Le Cabec, S. Benazzi, K. Harvati, P. Gunz, New fossils from Jebel Irhoud, Morocco and the pan-African origin of Homo sapiens. *Nature* **546**, 289–292 (2017). doi:10.1038/nature22336 Medline

2. D. Richter, R. Grün, R. Joannes-Boyau, T. E. Steele, F. Amani, M. Rué, P. Fernandes, J.-P. Raynal, D. Geraads, A. Ben-Ncer, J.-J. Hublin, S. P. McPherron, The age of the hominin fossils from Jebel Irhoud, Morocco, and the origins of the Middle Stone Age. *Nature* **546**, 293–296 (2017). doi:10.1038/nature22335 Medline

3. T. D. White, B. Asfaw, D. DeGusta, H. Gilbert, G. D. Richards, G. Suwa, F. C. Howell, Pleistocene homo sapiens from Middle Awash, Ethiopia. *Nature* **423**, 742–747 (2003). doi:10.1038/nature01669 Medline

4. I. McDougall, F. H. Brown, J. G. Fleagle, Stratigraphic placement and age of modern humans from Kibish, Ethiopia. *Nature* **433**, 733–736 (2005). doi:10.1038/nature03258 Medline

5. N. Mercier, H. Valladas, O. Bar-Yosef, B. Vandermeersch, C. Stringer, J.-L. Joron, Thermoluminescence date for the Mousterian burial site of Es-Skhul, Mt. Carmel. *J. Archaeol. Sci.* **20**, 169–174 (1993). doi:10.1006/jasc.1993.1012

6. C. B. Stringer, R. Grün, H. P. Schwarcz, P. Goldberg, ESR dates for the hominid burial site of Es Skhul in Israel. *Nature* **338**, 756–758 (1989). doi:10.1038/338756a0 Medline

7. H. P. Schwarcz, R. Grün, B. Vandermeersch, O. Bar-Yosef, H. Valladas, E. Tchernov, ESR dates for the hominid burial site of Qafzeh in Israel. *J. Hum. Evol.* **17**, 733–737 (1988). doi:10.1016/0047-2484(88)90063-2

8. W. Liu, M. Martinón-Torres, Y. J. Cai, S. Xing, H. W. Tong, S. W. Pei, M. J. Sier, X. H. Wu, R. L. Edwards, H. Cheng, Y. Y. Li, X. X. Yang, J. M. B. de Castro, X. J. Wu, The earliest unequivocally modern humans in southern China. *Nature* **526**, 696–699 (2015). doi:10.1038/nature15696 Medline

9. Materials and methods are available as supplementary materials at *Science* online.

10. Y. Zaidner, M. Weinstein-Evron, Making a point: The Early Middle Palaeolithic tool assemblage of Misliya Cave, Mount Carmel, Israel. *Before Farm.* **2012**, 1–23 (2012). doi:10.3828/bfarm.2012.4.1

11. H. Valladas, N. Mercier, I. Hershkovitz, Y. Zaidner, A. Tsatskin, R. Yeshurun, L. Vialettes, J.-L. Joron, J.-L. Reyss, M. Weinstein-Evron, Dating the Lower to Middle Paleolithic transition in the Levant: A view from Misliya Cave, Mount Carmel, Israel. *J. Hum. Evol.* **65**, 585–593 (2013). doi:10.1016/j.jhevol.2013.07.005 Medline

12. N. Mercier, H. Valladas, L. Froget, J.-L. Joron, J.-L. Reyss, S. Weiner, P. Goldberg, L. Meignen, O. Bar-Yosef, A. Belfer-Cohen, M. Chech, S. L. Kuhn, M. C. Stiner, A.-M. Tillier, B. Arensburg, B. Vandermeersch, Hayonim Cave: A TL-based chronology for this Levantine Mousterian sequence. *J. Archaeol. Sci.* **34**, 1064–1077 (2007). doi:10.1016/j.jas.2006.09.021

13. N. Mercier, H. Valladas, Reassessment of TL age estimates of burnt flints from the Paleolithic site of Tabun Cave, Israel. *J. Hum. Evol.* **45**, 401–409 (2003). doi:10.1016/j.jhevol.2003.09.004 Medline

14. M. Martinón-Torres, J. M. Bermúdez de Castro, A. Gómez-Robles, J. L. Arsuaga, E. Carbonell, D. Lordkipanidze, G. Manzi, A. Margvelashvili, Dental evidence on the hominin dispersals during the Pleistocene. *Proc. Natl. Acad. Sci. U.S.A.* **104**, 13279–13282 (2007). doi:10.1073/pnas.0706152104 Medline

15. F. Weidenreich. *The dentition of* Sinanthropus pekinensis*; a comparative odontography of the hominids. Palaeontol Sinica, New Series D1* (Peking, 1937).

16. S. E. Bailey, A morphometric analysis of maxillary molar crowns of Middle-Late Pleistocene hominins. *J. Hum. Evol.* **47**, 183–198 (2004). doi:10.1016/j.jhevol.2004.07.001 Medline

17. M. Martinón-Torres, J. M. Bermúdez de Castro, A. Gómez-Robles, L. Prado-Simón, J. L. Arsuaga, Morphological description and comparison of the dental remains from Atapuerca-Sima de los Huesos site (Spain). *J. Hum. Evol.* **62**, 7–58 (2012). doi:10.1016/j.jhevol.2011.08.007 Medline

18. J. M. Bermúdez de Castro, M. E. Nicolas, Posterior dental size reduction in hominids: The Atapuerca evidence. *Am. J. Phys. Anthropol.* **96**, 335–356 (1995). doi:10.1002/ajpa.1330960403 Medline

19. S. E. Bailey, J. Hublin, in *Anthropological Perspectives on Tooth Morphology: Genetics, Evolution, Variation*, G. Scott, J. Irish, Eds. (Cambridge Univ. Press, Cambridge, 2013), pp. 222–249.

20. G. Weber, C. Fornai, A. Gopher, R. Barkai, R. Sarig, I. Hershkovitz, The Qesem cave hominin material (Part 1): A morphometric analysis of the mandibular premolars and molar. *Quat. Int.* **398**, 159–174 (2016). doi:10.1016/j.quaint.2015.10.027

21. I. Hershkovitz, P. Smith, R. Sarig, R. Quam, L. Rodríguez, R. García, J. L. Arsuaga, R. Barkai, A. Gopher, Middle pleistocene dental remains from Qesem Cave (Israel). *Am. J. Phys. Anthropol.* **144**, 575–592 (2011). doi:10.1002/ajpa.21446 Medline

22. S. E. Freidline, P. Gunz, I. Janković, K. Harvati, J.-J. Hublin, A comprehensive morphometric analysis of the frontal and zygomatic bone of the Zuttiyeh fossil from Israel. *J. Hum. Evol.* **62**, 225–241 (2012). doi:10.1016/j.jhevol.2011.11.005 Medline

23. A. Gómez-Robles, J. M. Bermúdez de Castro, J.-L. Arsuaga, E. Carbonell, P. D. Polly, No known hominin species matches the expected dental morphology of the last common ancestor of Neanderthals and modern humans. *Proc. Natl. Acad. Sci. U.S.A.* **110**, 18196–18201 (2013). doi:10.1073/pnas.1302653110 Medline

24. C. Stringer, The origin and evolution of Homo sapiens. *Philos. Trans. R. Soc. Lond. B Biol. Sci.* **371**, 1698 (2016). Medline

25. J. L. Arsuaga, I. Martínez, L. J. Arnold, A. Aranburu, A. Gracia-Téllez, W. D. Sharp, R. M. Quam, C. Falguères, A. Pantoja-Pérez, J. Bischoff, E. Poza-Rey, J. M. Parés, J. M. Carretero, M. Demuro, C. Lorenzo, N. Sala, M. Martinón-Torres, N. García, A. Alcázar de Velasco, G. Cuenca-Bescós, A. Gómez-Olivencia, D. Moreno, A. Pablos, C.-C. Shen, L. Rodríguez, A. I. Ortega, R. García, A. Bonmatí, J. M. Bermúdez de Castro, E.

Carbonell, Neandertal roots: Cranial and chronological evidence from Sima de los Huesos. *Science* **344**, 1358–1363 (2014). doi:10.1126/science.1253958 Medline

26. S. E. Bailey, T. D. Weaver, J. Hublin, in *Human Paleontology and Prehistory*, A. Marom, E. Hovers, Eds. (Springer International, Cham, Switzerland, 2017), pp. 215–232.

27. G. Shen, W. Wang, Q. Wang, J. Zhao, K. Collerson, C. Zhou, P. V. Tobias, U-Series dating of Liujiang hominid site in Guangxi, Southern China. *J. Hum. Evol.* **43**, 817–829 (2002). doi:10.1006/jhev.2002.0601 Medline

28. W. Liu, X. Wu, L. Wang, Some problems for the Late Pleistocene human cranium found in Liujiang of South China based on morphological analysis. *Acta Anthropol. Sin.* **25**, 177–194 (2006).

29. M. Weinstein-Evron, Y. Zaidner, A. Tsatskin, R. Yeshurun, I. Hershkovitz, in *Quaternary of the Levant: Environments, Climate Change, and Humans*, Y. Enzel, O. Bar-Yosef, Eds. (Cambridge Univ. Press, Cambridge, 2017), pp. 225–230.

30. K. Douze, A. Delagnes, The pattern of emergence of a Middle Stone Age tradition at Gademotta and Kulkuletti (Ethiopia) through convergent tool and point technologies. *J. Hum. Evol.* **91**, 93–121 (2016). doi:10.1016/j.jhevol.2015.11.006 Medline

31. C. R. Johnson, S. McBrearty, 500,000 year old blades from the Kapthurin Formation, Kenya. *J. Hum. Evol.* **58**, 193–200 (2010). doi:10.1016/j.jhevol.2009.10.001 Medline

32. N. Porat, M. Chazan, R. Grün, M. Aubert, V. Eisenmann, L. K. Horwitz, New radiometric ages for the Fauresmith industry from Kathu Pan, southern Africa: Implications for the Earlier to Middle Stone Age transition. *J. Archaeol. Sci.* **37**, 269–283 (2010). doi:10.1016/j.jas.2009.09.038

33. Y. Sahle, L. E. Morgan, D. R. Braun, B. Atnafu, W. K. Hutchings, Chronological and behavioral contexts of the earliest Middle Stone Age in the Gademotta formation, main Ethiopian rift. *Quat. Int.* **331**, 6–19 (2014). doi:10.1016/j.quaint.2013.03.010

34. C. A. Tryon, S. McBrearty, P.-J. Texier, Levallois lithic technology from the Kapthurin formation, Kenya: Acheulian origin and Middle Stone Age diversity. *Afr. Archaeol. Rev.* **22**, 199–229 (2005). doi:10.1007/s10437-006-9002-5

35. I. Hershkovitz, O. Marder, A. Ayalon, M. Bar-Matthews, G. Yasur, E. Boaretto, V. Caracuta, B. Alex, A. Frumkin, M. Goder-Goldberger, P. Gunz, R. L. Holloway, B. Latimer, R. Lavi, A. Matthews, V. Slon, D. B.-Y. Mayer, F. Berna, G. Bar-Oz, R. Yeshurun, H. May, M. G. Hans, G. W. Weber, O. Barzilai, Levantine cranium from Manot Cave (Israel) foreshadows the first European modern humans. *Nature* **520**, 216–219 (2015). doi:10.1038/nature14134 Medline

36. C. Posth, C. Wißing, K. Kitagawa, L. Pagani, L. van Holstein, F. Racimo, K. Wehrberger, N. J. Conard, C. J. Kind, H. Bocherens, J. Krause, Deeply divergent archaic mitochondrial genome provides lower time boundary for African gene flow into Neanderthals. *Nat. Commun.* **8**, 16046 (2017). doi:10.1038/ncomms16046 Medline

37. C. O. Lovejoy, Dental wear in the Libben population: Its functional pattern and role in the determination of adult skeletal age at death. *Am. J. Phys. Anthropol.* **68**, 47–56 (1985). doi:10.1002/ajpa.1330680105 Medline

38. J. K. Ginter, A test of the effectiveness of the revised maxillary suture obliteration method in estimating adult age at death. *J. Forensic Sci.* **50**, 1303–1309 (2005). doi:10.1520/JFS2004520 Medline

39. R. Quam, S. Bailey, B. Wood, Evolution of M1 crown size and cusp proportions in the genus Homo. *J. Anat.* **214**, 655–670 (2009). doi:10.1111/j.1469-7580.2009.01064.x Medline

40. M. Martinón-Torres, P. Spěváčková, A. Gracia-Téllez, I. Martínez, E. Bruner, J. L. Arsuaga, J. M. Bermúdez de Castro, Morphometric analysis of molars in a Middle Pleistocene population shows a mosaic of 'modern' and Neanderthal features. *J. Anat.* **223**, 353–363 (2013). doi:10.1111/joa.12090 Medline

41. C. Turner, C. Nichol, G. Scott, in *Advances in Dental Anthropology 1*, C. Larsen, Ed. (Wiley-Liss, New-York, 1991), pp. 13–31.

42. R. Martin, *Lehrbuch der Anthropologie in systematischer Darstellung: Bd. Bibliographie, literaturverzeichnis, sachregister, autorenregister* (G. Fischer, 1928), vol. 3.

43. B. A. Wood, C. A. Engleman, Analysis of the dental morphology of Plio-Pleistocene hominids. V. Maxillary postcanine tooth morphology. *J. Anat.* **161**, 1–35 (1988). Medline

44. A. Le Cabec, P. Gunz, K. Kupczik, J. Braga, J.-J. Hublin, Anterior tooth root morphology and size in Neanderthals: Taxonomic and functional implications. *J. Hum. Evol.* **64**, 169–193 (2013). doi:10.1016/j.jhevol.2012.08.011 Medline

45. G. W. Weber, F. L. Bookstein, *Virtual Anthropology: A Guide to a New Interdisciplinary Field* (Springer, 2011).

46. G. W. Weber, V. A. Krenn, Zygomatic root position in recent and fossil hominids. *Anat. Rec.* **300**, 160–170 (2017). doi:10.1002/ar.23490 Medline

47. S. Benazzi, C. Fornai, L. Buti, M. Toussaint, F. Mallegni, S. Ricci, G. Gruppioni, G. W. Weber, S. Condemi, A. Ronchitelli, Cervical and crown outline analysis of worn Neanderthal and modern human lower second deciduous molars. *Am. J. Phys. Anthropol.* **149**, 537–546 (2012). doi:10.1002/ajpa.22155 Medline

48. S. Molnar, Human tooth wear, tooth function and cultural variability. *Am. J. Phys. Anthropol.* **34**, 175–189 (1971). doi:10.1002/ajpa.1330340204 Medline

49. J. C. Gower, Generalized procrustes analysis. *Psychometrika* **40**, 33–51 (1975). doi:10.1007/BF02291478

50. L. F. Marcus, M. Corti, A. Loy, G. Naylor, D. E. Slice, *Advances in Morphometrics* (Plenum, New York, 1996).

51. S. M. Eggins, R. Grün, M. T. McCulloch, A. W. G. Pike, J. Chappell, L. Kinsley, G. Mortimer, M. Shelley, C. V. Murray-Wallace, C. Spötl, L. Taylor, In situ U-series dating by laser-ablation multi-collector ICPMS: New prospects for Quaternary geochronology. *Quat. Sci. Rev.* **24**, 2523–2538 (2005). doi:10.1016/j.quascirev.2005.07.006

52. R. Grün, S. Eggins, L. Kinsley, H. Moseley, M. Sambridge, Laser ablation U-series analysis of fossil bones and teeth. *Palaeogeogr. Palaeoclimatol. Palaeoecol.* **416**, 150–167 (2014). doi:10.1016/j.palaeo.2014.07.023

53. R. Grün, R. Joannes-Boyau, C. Stringer, Two types of CO_2^- radicals threaten the fundamentals of ESR dating of tooth enamel. *Quat. Geochronol.* **3**, 150–172 (2008). doi:10.1016/j.quageo.2007.09.004

54. M. Duval, R. Grün, Are published ESR dose assessments on fossil tooth enamel reliable? *Quat. Geochronol.* **31**, 19–27 (2016). doi:10.1016/j.quageo.2015.09.007

55. R. Grün, O. Katzenberger-Apel, An alpha irradiator for ESR dating. *Anc. TL* **12**, 35–38 (1994).

56. R. E. Marsh, "Beta-gradient isochrons using electron paramagnetic resonance: Towards a new dating method in archaeology," thesis, McMaster University, Hamilton (1999).

57. G. Adamiec, M. J. Aitken, Dose-rate conversion factors: Update. *Anc. TL* **16**, 37–50 (1998).

58. R. Grün, Alpha dose attenuation in thin layers. *Anc. TL* **5**, 6–8 (1987).

59. Q. Shao, J.-J. Bahain, J.-M. Dolo, C. Falguères, Monte Carlo approach to calculate US-ESR age and age uncertainty for tooth enamel. *Quat. Geochronol.* **22**, 99–106 (2014). doi:10.1016/j.quageo.2014.03.003

60. R. Joannes-Boyau, R. Grün, A comprehensive model for CO_2^- radicals in fossil tooth enamel: Implications for ESR dating. *Quat. Geochronol.* **6**, 82–97 (2011). doi:10.1016/j.quageo.2010.09.001

61. R. Joannes-Boyau, Detailed protocol for an accurate non-destructive direct dating of tooth enamel fragment using Electron Spin Resonance. *Geochronometria* **40**, 322–333 (2013). doi:10.2478/s13386-013-0132-7

62. M. Duval, L. Martín-Francés, Quantifying the impact of µCT-scanning of human fossil teeth on ESR age results. *Am. J. Phys. Anthropol.* **163**, 205–212 (2017). doi:10.1002/ajpa.23180 Medline

63. A. Kaufman, G. J. Wasserburg, D. Porcelli, M. Bar-Matthews, A. Ayalon, L. Halicz, U-Th isotope systematics from the Soreq cave, Israel and climatic correlations. *Earth Planet. Sci. Lett.* **156**, 141–155 (1998). doi:10.1016/S0012-821X(98)00002-8

64. D. A. Richards, J. A. Dorale, Uranium-series chronology and environmental applications of speleothems. *Rev. Mineral. Geochemistry*. **52**, 407–460 (2003).

65. K. R. Ludwig, D. M. Titterington, Calculation of ^{230}ThU isochrons, ages, and errors. *Geochim. Cosmochim. Acta* **58**, 5031–5042 (1994). doi:10.1016/0016-7037(94)90229-1

66. J. Daura, M. Sanz, J. L. Arsuaga, D. L. Hoffmann, R. M. Quam, M. C. Ortega, E. Santos, S. Gómez, A. Rubio, L. Villaescusa, P. Souto, J. Mauricio, F. Rodrigues, A. Ferreira, P. Godinho, E. Trinkaus, J. Zilhão, New Middle Pleistocene hominin cranium from Gruta da Aroeira (Portugal). *Proc. Natl. Acad. Sci. U.S.A.* **114**, 3397–3402 (2017). doi:10.1073/pnas.1619040114 Medline

67. G. P. Rightmire, Evidence from facial morphology for similarity of Asian and African representatives of *Homo erectus*. *Am. J. Phys. Anthropol.* **106**, 61–85 (1998). doi:10.1002/(SICI)1096-8644(199805)106:1<61:AID-AJPA5>3.0.CO;2-G Medline

68. F. Weidenreich, *The Skull of* Sinanthropus pekinensis*: A Comparative Study on a Primitive Hominid Skull* (Geological Survey of China, 1943).

69. J. L. Heim, Les Hommes Fossiles de La Ferrassie. Tome I. Le gisement, les squelettes adultes (crâne et squelette du tronc) Archives de L'Institut de Paléontologie Humaine, mémoire 35 (1976).

70. H. Martin, *L'homme fossile de la Quina* (O. Doin, 1923), vol. 15.

71. J.-L. Arsuaga, I. Martínez, C. Lorenzo, A. Gracia, A. Muñoz, O. Alonso, J. Gallego, The human cranial remains from Gran Dolina lower Pleistocene site (Sierra de Atapuerca, Spain). *J. Hum. Evol.* **37**, 431–457 (1999). doi:10.1006/jhev.1999.0309 Medline

72. E. Trinkaus, The Neandertal face: Evolutionary and functional perspectives on a recent hominid face. *J. Hum. Evol.* **16**, 429–443 (1987). doi:10.1016/0047-2484(87)90071-6

73. E. Trinkaus, The Shanidar Neandertals. *J. Hum. Evol.* **16**, 429–443 (1983). doi:10.1016/0047-2484(87)90071-6

74. K. Harvati, E. N. Lopez, in *Human Paleontology and Prehistory*, A. Marom, E. Hovers, Eds. (Springer International, Cham, Switzerland, 2017), pp. 203–213.

75. R. G. Franciscus, Internal nasal floor configuration in *Homo* with special reference to the evolution of Neandertal facial form. *J. Hum. Evol.* **44**, 701–729 (2003). doi:10.1016/S0047-2484(03)00062-9 Medline

76. X.-J. Wu, S. D. Maddux, L. Pan, E. Trinkaus, Nasal floor variation among eastern Eurasian Pleistocene Homo. *Anthropol. Sci.* **120**, 217–226 (2012). doi:10.1537/ase.120709

77. S. E. Bailey, The evolution of non-metric dental variation in Europe. *Mitteilungen der Gesellschaft für Urgeschichte* **15**, 9–30 (2006).

78. S. Bailey, Beyond shovel-shaped incisors: Neandertal dental morphology in a comparative context. *Period. Biol.* **108**, 253–267 (2006).

79. F. Weidenreich, The new discovery of three skulls of Sinanthropus pekinensis. *Nature* **139**, 269–272 (1937). doi:10.1038/139269a0

80. S. E. Bailey, W. Liu, A comparative dental metrical and morphological analysis of a Middle Pleistocene hominin maxilla from Chaoxian (Chaohu), China. *Quat. Int.* **211**, 14–23 (2010). doi:10.1016/j.quaint.2009.01.008

81. W. Liu, L. A. Schepartz, S. Xing, S. Miller-Antonio, X. Wu, E. Trinkaus, M. Martinón-Torres, Late middle pleistocene hominin teeth from Panxian Dadong, South China. *J. Hum. Evol.* **64**, 337–355 (2013). doi:10.1016/j.jhevol.2012.10.012 Medline

82. W. Liu, X. Wu, S. Pei, X. Wu, C. J. Norton, Huanglong Cave: A late Pleistocene human fossil site in Hubei Province, China. *Quat. Int.* **211**, 29–41 (2010). doi:10.1016/j.quaint.2009.06.017

83. S. Xing, M. Martinón-Torres, J. M. Bermúdez de Castro, X. Wu, W. Liu, Hominin teeth from the early Late Pleistocene site of Xujiayao, Northern China. *Am. J. Phys. Anthropol.* **156**, 224–240 (2015). doi:10.1002/ajpa.22641 Medline

84. S. Xing, M. Martinón-Torres, J. M. Bermúdez de Castro, Y. Zhang, X. Fan, L. Zheng, W. Huang, W. Liu, Middle Pleistocene hominin teeth from Longtan Cave, Hexian, China. *PLOS ONE* **9**, e114265 (2014). doi:10.1371/journal.pone.0114265 Medline

85. Z. Lu, in *Current Research in Chinese Pleistocene Archaeology*, C. Shen, S. Keates, Eds. (BAR Archaeopress, Oxford, 2003), pp. 127–136.

86. J. L. Arsuaga, J. Fernández Peris, A. Gracia-Téllez, R. Quam, J. M. Carretero, V. Barciela González, R. Blasco, F. Cuartero, P. Sañudo, Fossil human remains from Bolomor Cave (Valencia, Spain). *J. Hum. Evol.* **62**, 629–639 (2012). doi:10.1016/j.jhevol.2012.02.002 Medline

87. T. Higham, T. Compton, C. Stringer, R. Jacobi, B. Shapiro, E. Trinkaus, B. Chandler, F. Gröning, C. Collins, S. Hillson, P. O'Higgins, C. FitzGerald, M. Fagan, The earliest evidence for anatomically modern humans in northwestern Europe. *Nature* **479**, 521–524 (2011). doi:10.1038/nature10484 Medline

88. I. Hershkovitz, G. W. Weber, C. Fornai, A. Gopher, R. Barkai, V. Slon, R. Quam, Y. Gabet, R. Sarig, New Middle Pleistocene dental remains from Qesem Cave (Israel). *Quat. Int.* **398**, 148–158 (2016). doi:10.1016/j.quaint.2015.08.059

89. P. J. Macaluso Jr., Variation in dental remains from Dmanisi, Georgia. *Anthropol. Sci.* **118**, 31–40 (2010). doi:10.1537/ase.090501

90. A. Gómez-Robles, J. M. B. de Castro, M. Martinón-Torres, L. Prado-Simón, Crown size and cusp proportions in Homo antecessor upper first molars. A comment on Quam et al. 2009. *J. Anat.* **218**, 258–262 (2011). doi:10.1111/j.1469-7580.2010.01324.x Medline

91. S. Bailey, M. Glantz, T. D. Weaver, B. Viola, The affinity of the dental remains from Obi-Rakhmat Grotto, Uzbekistan. *J. Hum. Evol.* **55**, 238–248 (2008). doi:10.1016/j.jhevol.2008.03.004 Medline

92. J. Hublin, C. Verna, S. Bailey, T. Smith, A. Olejniczak, F. Z. Sbihi-Alaoui, M. Zouak, in *Modern Origins: A North African Perspective*, J. Hublin, Ed. (Springer, Dordrecht, 2012), pp. 189–204.

93. G. A. Macho, J. Moggi-Cecchi, Reduction of maxillary molars in Homo sapiens sapiens: A different perspective. *Am. J. Phys. Anthropol.* **87**, 151–159 (1992). doi:10.1002/ajpa.1330870203 Medline

94. S. E. Bailey, in *Current Trends in Dental Morphology Research*, E. Zadzinska, Ed. (University of Łódź Press, Łódź, 2005), pp. 201–210.

95. D. A. Garrod, D. M. A. Bate, *The Stone Age of Mount Carmel*, vol. 1, *Excavations at the Wady El-Mughara* (1937).

96. A. J. Jelinek, W. R. Farrand, G. Haas, A. Horowitz, P. Goldberg, New excavations at the Tabun Cave, Mount Carmel, Israel, 1967-1972: A preliminary report. *Paéorient* •••, 151–183 (1973).

97. T. D. McCown, Mugharet es-Skhul. Description and excavations. *Stone Age Mt. Carmel* **1**, 91–112 (1937).

98. M. Weinstein-Evron, A. Tsatskin, The Jamal cave is not empty: Recent discoveries in the Mount Carmel caves, Israel. *Paéorient* •••, 119–128 (1994).

99. Y. Zaidner, D. Druck, M. Nadler, M. Weinstein-Evron, The Acheulo-Yabrudian of Jamal Cave, Mount Carmel, Israel. *Mitekufat Haeven J. Isr. Prehist. Soc.* **35**, 93–115 (2005).

100. O. Bar-Yosef, B. Vandermeersch, B. Arensburg, A. Belfer-Cohen, P. Goldberg, H. Laville, L. Meignen, Y. Rak, J. D. Speth, E. Tchernov, S. Weiner, G. A. Clark, A. Garrard, D. O. Henry, F. Hole, D. Roe, K. R. Rosenberg, L. A. Schepartz, J. J. Shea, F. H. Smith, E. Trinkaus, N. M. Whalen, L. Wilson, The excavations in Kebara Cave, Mt. Carmel [and comments and replies]. *Curr. Anthropol.* **33**, 497–550 (1992). doi:10.1086/204112

101. M. Weinstein-Evron, G. Bar-Oz, Y. Zaidner, A. Tsatskin, D. Druck, N. Porat, I. Hershkovitz, Introducing Misliya Cave, Mount Carmel, Israel: A new continuous Lower/Middle Paleolithic sequence in the Levant. *Eurasian Prehistory* **1**, 31–55 (2003).

102. Y. Zaidner, D. Druck, M. Weinstein-Evron, in *Axe Age: Acheulian Toolmaking - from Quarry to Discard*, N. Goren-Inbar, G. Sharon, Eds. (Equinox, Oxford, 2006).

103. Y. Zaidner, M. Weinstein-Evron, The end of the Lower Paleolithic in the Levant: The acheulo-yabrudian lithic technology at Misliya cave, Israel. *Quat. Int.* **409**, 9–22 (2016). doi:10.1016/j.quaint.2015.12.080

104. M. Weinstein-Evron, A. Tsatskin, S. Weiner, R. Shahack-Gross, A. Frumkin, R. Yeshurun, Y. Zaidner, A Window into Early Middle Paleolithic human occupational layers: Misliya Cave, Mount Carmel, Israel. *Paleoanthropology* **2012**, 202–228 (2012).

105. R. Yeshurun, G. Bar-Oz, M. Weinstein-Evron, Modern hunting behavior in the early Middle Paleolithic: Faunal remains from Misliya Cave, Mount Carmel, Israel. *J. Hum. Evol.* **53**, 656–677 (2007). doi:10.1016/j.jhevol.2007.05.008 Medline

106. I. Groman-Yaroslavski, Y. Zaidner, M. Weinstein-Evron, Mousterian Abu Sif points: Foraging tools of the Early Middle Paleolithic site of Misliya Cave, Mount Carmel, Israel. *J. Archaeol. Sci. Rep.* **7**, 312–323 (2016). doi:10.1016/j.jasrep.2016.05.002

107. A. Yaroshevich, Y. Zaidner, M. Weinstein-Evron, in *Multidisciplinary Approaches to the Study of Stone Age Weaponry*, R. Iovita, K. Sano, Eds. (Springer, Dordrecht, 2016), pp. 119–134.

108. J. M. Bermudez de Castro, The Atapuerca dental remains – new evidence (1987-1991 Excavations) and interpretations. *J. Hum. Evol.* **24**, 339–371 (1993). doi:10.1006/jhev.1993.1027

109. T. D. McCown, A. Keith, *The Stone Age of Mount Carmel* (Clarendon, Oxford, 1939), vol. 2.

110. B. Vandermeersch, *Les Hommes Fossiles de Qafzeh (Israel)*. (CNRS, Paris, 1981).

111. A. M. Tillier, *Les enfants moustériens de Qafzeh: Interprétation phylogénétique et paléoauxologique.* Cahiers de Paléoanthropologie (CNRS, Paris, 1999)

112. E. Vlcek, in *Pavlov I - Northwest. The Upper Paleolithic Burial and Its Settlement Context*, J. Svoboda, Ed. (ceská akademie vfd., Brno, 1997), pp. 53-153.

113. V. Sládek, E. Trinkaus, S. Hillson, T. Holliday, *The People of the Pavlovian. Skeletal Catalogue and Osteometrics of the Gravettian Fossil Hominids from Dolní Vestonice*. (Academy of Sciences of the Czech Republic, Brno, 2000).

114. E. Trinkaus, A. P. Buzhilova, M. B. Mednikova, M. V. Dobrovolskaya, *The People of Sunghir: Burials, Bodies, and Behavior in the Earlier Upper Paleolithic* (Oxford Univ. Press, New York, 2014).